



OH-initiated atmospheric degradation of hydroxyalkyl hydroperoxides: mechanism, kinetics, and structure–activity relationship

Long Chen^{1,2}, Yu Huang^{1,2}, Yonggang Xue^{1,2}, Zhihui Jia³, and Wenliang Wang⁴

¹State Key Lab of Loess and Quaternary Geology (SKLLQG), Institute of Earth Environment, Chinese Academy of Sciences (CAS), Xi'an, 710061, China

²CAS Center for Excellence in Quaternary Science and Global Change, Xi'an, 710061, China

³School of Materials Science and Engineering, Shaanxi Normal University, Xi'an, Shaanxi, 710119, China

⁴School of Chemistry and Chemical Engineering, Key Laboratory for Macromolecular Science of Shaanxi Province, Shaanxi Normal University, Xi'an, Shaanxi, 710119, China

Correspondence: Yu Huang (huangyu@ieecas.cn)

Received: 25 October 2021 – Discussion started: 8 November 2021

Revised: 9 February 2022 – Accepted: 15 February 2022 – Published: 18 March 2022

Abstract. Hydroxyalkyl hydroperoxides (HHPs), formed in the reactions of Criegee intermediates (CIs) with water vapor, play essential roles in the formation of secondary organic aerosol (SOA) under atmospheric conditions. However, the transformation mechanisms for the OH-initiated oxidation of HHPs remain incompletely understood. Herein, the quantum chemical and kinetics modeling methods are applied to explore the mechanisms of the OH-initiated oxidation of the distinct HHPs (HOCH_2OOH , $\text{HOCH}(\text{CH}_3)\text{OOH}$, and $\text{HOC}(\text{CH}_3)_2\text{OOH}$) formed from the reactions of CH_2OO , *anti*- CH_3CHOO , and $(\text{CH}_3)_2\text{COO}$ with water vapor. The calculations show that the dominant pathway is H-abstraction from the -OOH group in the initiation reactions of the OH radical with HOCH_2OOH and $\text{HOC}(\text{CH}_3)_2\text{OOH}$. H-abstraction from the -CH group is competitive with that from the -OOH group in the reaction of the OH radical with $\text{HOCH}(\text{CH}_3)\text{OOH}$. The barrier of H-abstraction from the -OOH group slightly increases when the number of methyl groups increase. In pristine environments, the self-reaction of the RO_2 radical initially produces a tetroxide intermediate via oxygen-to-oxygen coupling, and then it decomposes into propagation and termination products through asymmetric two-step O–O bond scission, in which the rate-limiting step is the first O–O bond cleavage. The barrier height of the reactions of distinct RO_2 radicals with the HO_2 radical is not affected by the number of methyl substitutions. In urban environments, the reaction with O_2 to form formic acid and the HO_2 radical is the dominant removal pathway for the HOCH_2O radical formed from the reaction of the HOCH_2OO radical with NO. The β -site C–C bond scission is the dominant pathway in the dissociation of the $\text{HOCH}(\text{CH}_3)\text{O}$ and $\text{HOC}(\text{CH}_3)_2\text{O}$ radicals formed from the reactions of NO with $\text{HOCH}(\text{CH}_3)\text{OO}$ and $\text{HOC}(\text{CH}_3)_2\text{OO}$ radicals. These new findings deepen our understanding of the photochemical oxidation of hydroperoxides under realistic atmospheric conditions.

1 Introduction

Hydroxyalkyl hydroperoxides (HHPs), formed in the reactions of Criegee intermediates (CIs) with water vapor and in the initiation OH-addition with subsequent HO₂-termination reactions, play important roles in the formation of secondary organic aerosol (SOA; Qiu et al., 2019; Kumar et al., 2014). The CIs formed from the ozonolysis of alkenes are characterized by high reactivity and excess energy, which can either prompt the unimolecular decay to an OH radical or, after collisional stabilization, bimolecular reactions with various trace gases such as SO₂, NO₂, and H₂O to produce sulfate, nitrate, and SOA, thereby influencing air quality and human health (Lester and Klippenstein, 2018; Chen et al., 2017, 2019; Liu et al., 2019; Chhantyal-Pun et al., 2017; Anglada and Solé, 2016; Gong and Chen, 2021). Among these reactions, the bimolecular reaction of CIs with water is regarded as the dominant chemical sink, since its concentration ($1.3\text{--}8.3 \times 10^{17}$ molecules cm⁻³) is several orders of magnitude greater than those of SO₂ and NO₂ ($\sim 10^{12}$ molecules cm⁻³) in the atmosphere (Huang et al., 2015; Khan et al., 2018; Taatjes et al., 2013; Taatjes, 2017). The primary products of the reaction of CIs with water are highly oxygenated HHPs, which are difficult to detect and identify through the available analytical techniques because of their thermal instability (Qiu et al., 2019; Anglada and Solé, 2016; Chao et al., 2015; Chen et al., 2016a; Ryzhkov and Ariya, 2003).

Due to the presence of both hydroxyl and perhydroxy moieties, HHPs have relatively low volatility and contribute significantly to the formation of SOA (Qiu et al., 2019). The atmospheric degradation of HHPs initiated by an OH radical is expected to be one of the dominant loss processes because the OH radical is a powerful oxidizing agent (Gligorovski et al., 2015; Allen et al., 2018). The reaction with the OH radical includes three possible H-abstraction channels, namely (a) alkyl hydrogen, (b) -OH hydrogen, and (c) -OOH hydrogen, which are followed by further reactions to generate organic peroxy radicals (RO₂) as reactive intermediates (Allen et al., 2018). On the basis of our current mechanistic understanding, RO₂ radicals have three possible channels in pristine environments: (1) RO₂ radicals can proceed self- and cross-reactions to generate the alkoxy radical RO, alcohol, carbonyl, and accretion products (Berndt et al., 2018; Zhang et al., 2012; Valiev et al., 2019); (2) RO₂ radicals can react with the HO₂ radical to form closed-shell hydroperoxide (ROOH), an RO radical, an OH radical, etc. (Dillon and Crowley, 2008; Iyer et al., 2018); (3) RO₂ radicals can undergo autooxidation through intramolecular H-shift and alternating O₂-addition steps to produce highly oxygenated organic molecules (HOMs), which have been identified as low volatility compounds that contribute to the formation of SOA (Crounse et al., 2013; Jokinen et al., 2014; Wang et al., 2018; Ehn et al., 2014; Iyer et al., 2021). In urban environments, RO₂ radicals can react with NO_x to generate peroxyxynitrate (RO₂NO₂), organic nitrate (RONO₂), RO radicals, and other

SOA precursors (Wang et al., 2017; Xu et al., 2014, 2020; Ma et al., 2021). The relative importance of distinct pathways is highly dependent on the nature of RO₂ radicals and the concentrations of coreactants.

Hydroxymethyl hydroperoxide (HMHP, HOCH₂OOH), the simplest HHP derived from the ozonolysis of all terminal alkenes in the presence of water, is observed in significant abundance in the atmosphere (Allen et al., 2018). The measured concentration of HMHP varies considerably depending on the location, season, and altitude, and its concentration has been reported to be as high as 5 ppbv in forested regions (Allen et al., 2018; Francisco and Eisfeld, 2009). In one study, the concentration of HMHP was measured during the summer of 2013 in the southeastern United States, and it was found that the average mixing ratio of HMHP was 0.25 ppbv with a maximum of 4.0 ppbv in the boundary layer (Allen et al., 2018). Allen et al. (2018) conducted the OH-initiated oxidation of HMHP in an environmental chamber and simulated the effect of HMHP oxidation on global formic acid production by applying the chemical transport model GEOS-Chem. They found that H-abstraction from the methyl group of HMHP results in the formation of formic acid and contributes approximately 1.7 Tg yr^{-1} to global formic acid production. Francisco and Eisfeld (2009) employed *ab initio* CCSD (T) and MP2 methods to study the atmospheric oxidation mechanism of HMHP initiated by the OH radical, and they also concluded that the degradation of HMHP can contribute to the formation of formic acid in the atmosphere. Additionally, the unimolecular decomposition of HMHP is another key removal process in the atmosphere. Chen et al. (2016b) found that the formation of CH₂O and H₂O₂ is more preferable than the production of HCOOH and H₂O. Kumar et al. (2014) also concluded that the aldehyde- or ketone-forming pathway is kinetically favored over the carboxylic acid-forming channel in the unimolecular decomposition of various HHPs. All of the above milestone investigations offer highly useful information on the decomposition of HHPs in the gas phase. However, to the best of our knowledge, there have been few studies on the subsequent transformations of the resulting H-abstraction products formed from the OH-initiated oxidation of larger HHPs. The effect of the size and number of substituents on the rates and outcomes of SOA precursors (e.g., ROOR, HOMs) is uncertain up to now. Therefore, it is necessary to evaluate the potential of larger HHPs and their oxidation products to substantial SOA formation under different NO_x conditions.

In the present study, the mechanisms and kinetics of distinct HHPs oxidation initiated by OH radicals are investigated by employing quantum chemical and kinetics modeling methods. For the resulting H-abstraction products of RO₂ radicals, the subsequent reactions involving self-reaction, isomerization, and reaction with HO₂ radicals are considered in the absence of NO, while the subsequent reactions including addition, decomposition, and H-abstraction by O₂ are considered in the presence of NO. The HHPs investigated

in the present study are generated from the bimolecular reactions of distinct carbonyl oxides (CH_2OO , *anti*- CH_3CHOO , and $(\text{CH}_3)_2\text{COO}$) with water vapor.

2 Computational details

2.1 Electronic structure and energy calculations

The equilibrium geometries of all open-shell species, including reactant (R), pre-reactive complex (RC), transition state (TS), post-reactive complex (PC), and product (P), are fully optimized at the unrestricted M06-2X/6-311+G(2df,2p) level of theory (UM06-2X; Zhao and Truhlar, 2006; Zheng and Truhlar, 2009), whereas all the closed-shell species are optimized at the restricted M06-2X/6-311+G(2df,2p) level of theory (RM06-2X). This is because the M06-2X functional has been proven to be reliable for describing thermochemistry, kinetics, and non-covalent interactions (Zhao and Truhlar, 2008). Harmonic vibrational frequencies are performed at the same level to verify that each stationary point is either a true minima (with no imaginary frequency) or a transition state (with one imaginary frequency). Zero-point vibrational energy (ZPVE) and Gibbs free-energy corrections (G_{corr}) from harmonic vibrational frequencies are scaled by a factor of 0.98 (Zhao and Truhlar, 2006). Intrinsic reaction coordinate (IRC) calculations are performed to verify the connection between the transition state and the designated reactant and product (Fukui, 1981). The single-point energies are calculated at the (U/R)M06-2X/ma-TZVP level of theory (Zheng et al., 2011).

The tetroxide intermediate formed from the self-reaction of the RO_2 radical proceeds through asymmetric two-step O–O bond scission to produce a caged tetroxide intermediate of overall singlet multiplicity comprising two same-spin alkoxy radicals (spin down) and triplet oxygen (spin up). This type of reaction mechanism can be described by broken symmetry unrestricted DFT (UDFT) and multi-reference CASSCF methods (Lee et al., 2016; Bach et al., 2005). Previous studies have demonstrated that the UDFT method is suitable for identifying the minimum of a metastable singlet caged radical complex and the transition state of O–O bond homolysis, and the resulting energies obtained using the UDFT method are comparable to those obtained using the more accurate and expensive CASSCF method (Lee et al., 2016; Bach et al., 2005). In the present study, the UDFT method, which provides a balance between computational accuracy and efficiency, is selected to study asymmetric O–O bond scission. The broken symmetry UM06-2X/6-311+G(2df,2p) method is applied to generate the initial guesses for the geometries of the tetroxide intermediate and transition state with mixed HOMO and LUMO ($S^2 \approx 1$) by using the guess = mix keyword. The single-point energies are refined at the UM06-2X/ma-TZVP level of theory.

To further evaluate the reliability of the employed method for predicting the reaction mechanisms, the single-point en-

ergies of all stationary points involved in the initiation reactions of OH radicals with distinct HHPs are recalculated at the (U/R)CCSD(T)/6-311+G(2df,2p) level of theory based on the (U/R)M06-2X optimized geometries. Furthermore, the stability of the pre-reactive complexes is assessed by performing basis set superposition error (BSSE) using the counterpoise method (Boys and Bernardi, 1970). For simplicity, no prefix is used throughout this article. Herein, the Gibbs free energy (G) for each species is obtained by combining the single-point energy with the Gibbs correction ($G = G_{\text{corr}} + E$). The electronic energy ($\Delta E_a^\#$) and free energy ($\Delta G_a^\#$) barriers are defined as the difference in energy between the transition state and pre-reactive complex ($\Delta E_a^\# = E_{\text{TS}} - E_{\text{RC}}$ and $\Delta G_a^\# = G_{\text{TS}} - G_{\text{RC}}$). The reaction free energy (ΔG) is referred to the difference in energy between the product and reactant ($\Delta G = G_{\text{P}} - G_{\text{R}}$). The calculated $\Delta E_a^\#$ and $\Delta G_a^\#$ for the initiation H-abstraction pathways are summarized in Table S1 in the Supplement. As shown in Table S1, the mean absolute deviations (MADs) of $\Delta E_a^\#$ and $\Delta G_a^\#$ between the CCSD(T)/6-311+G(2df,2p) and M06-2X/ma-TZVP approaches are 0.43 and 0.45 kcal mol^{−1}, respectively; the largest deviations of $\Delta E_a^\#$ and $\Delta G_a^\#$ are 1.2 and 1.1 kcal mol^{−1}, respectively. These results reveal that the energies obtained using the M06-2X/ma-TZVP method are in good accord with those obtained using the gold-standard coupled-cluster approach CCSD (T) within the uncertainties of systematic errors. Therefore, the M06-2X/ma-TZVP method is selected to investigate the atmospheric degradation of HHP initiated by OH radicals under different conditions. In the following sections, $\Delta G_a^\#$ is applied to construct the reaction profiles unless otherwise stated.

For the H-shift reactions of RO_2 radicals, reactants, transition states, and products have multiple conformers. Previous literature has demonstrated that the reaction kinetics of multi-conformer involvement are more precise than that of single-conformer approximation (Møller et al., 2016, 2020). Herein, the multi-conformer treatment is performed to investigate the H-shift reactions of RO_2 radicals. A conformer search within the Molclus program is employed to generate a pool of conformers for RO_2 radicals (Lu, 2020). The selected conformers are further optimized at the M06-2X/6-311+G(2df,2p) level of theory, followed by single-point energy calculations at the M06-2X/ma-TZVP level of theory. On the basis of the calculated Gibbs free energies, the Boltzmann populations (w_i) of each RO_2 conformer are expressed as Eq. (1):

$$w_i = \frac{e^{-\Delta G_i/k_B T}}{\sum_i e^{-\Delta G_i/k_B T}}, \quad (1)$$

where ΔG_i is the relative Gibbs free energy of conformer i , k_B is Boltzmann's constant, and T is temperature in Kelvin. All the quantum chemical calculations are performed by using the Gaussian 09 program (Frisch et al., 2009).

2.2 Kinetics calculations

The rate coefficients of unimolecular reactions are calculated by using the Rice–Ramsperger–Kassel–Marcus theory coupled with the energy-grained master equation (RRKM-ME) method (Holbrook et al., 1996), and the rate coefficients of bimolecular reactions are determined by utilizing traditional transition state theory (TST; Fernández-Ramos et al., 2007). RRKM-ME calculations are performed by using the MESMER 6.0 program (Glowacki et al., 2012). N₂ is used as the buffer gas. A single exponential down model is employed to simulate the collision energy transfer ($\langle\Delta E\rangle_{\text{down}} = 200 \text{ cm}^{-1}$). The collisional Lennard-Jones parameters are estimated by using an empirical formula proposed by Gilbert and Smith (1990). For the H-shift reactions of RO₂ radicals, the rate coefficients are determined by employing the multi-conformer transition state theory (MC-TST) approach (Møller et al., 2016). The MC-TST rate coefficient $k_{\text{MC-TST}}$ is calculated by the sum of individual intrinsic reaction coordinate TST (IRC-TST) rate coefficient $k_{\text{IRC-TST}}$, each weighted by the Boltzmann population of the corresponding RO₂ conformer (Møller et al., 2016):

$$k_{\text{MC-TST}} = \sum_i^{\text{all TS conf.}} w_i \times k_{\text{IRC-TST}i}, \quad (2)$$

where $k_{\text{IRC-TST}i}$ represents the rate coefficient of conformer i , and w_i is the relative Boltzmann population of the corresponding reactant connected to TS _{i} . The one-dimensional asymmetry Eckart model is employed to calculate the tunneling correction (Eckart, 1930). Considering the uncertainty in barrier heights ($\sim 1.0 \text{ kcal mol}^{-1}$ by the M06-2X method) and in tunneling corrections, the uncertainty of the calculated rate coefficient is about 1 order of magnitude in the present study.

3 Results and discussion

3.1 Initiation reaction of HHPs with an OH radical

Previous literatures have proposed that the lifetime of CI with respect to the reaction with water vapor exhibits strong dependence on the nature of CI (Anglada and Solé, 2016; Taatjes et al., 2013; Anglada et al., 2011), and the primary product is HHPs in both the gas phase and air–water interfaces (Chao et al., 2015; Chen et al., 2016a; Smith et al., 2015; Zhu et al., 2016; Zhong et al., 2018). In the present study, we mainly consider three kinds of HHPs originating from the addition of water to CH₂OO and methyl-substituted CI (*anti*-CH₃CHOO and (CH₃)₂COO). The lowest-energy HHP conformers (HOCH₂OOH, HOCH(CH₃)OOH, and HOC(CH₃)₂OOH) are obtained from a previous study, as shown in Fig. 1 (Chen et al., 2019), and they are selected as the model system to investigate the atmospheric degradation mechanism of HHP initiated by the OH radical. Letters

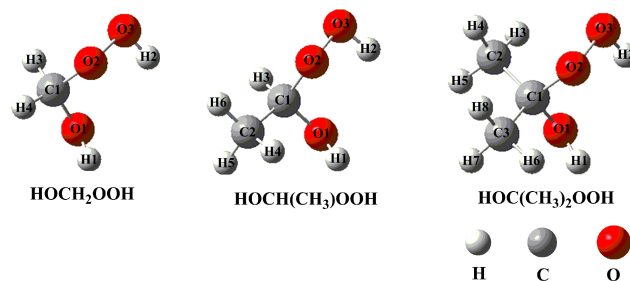


Figure 1. The structures of distinct HHPs.

and numbers are used to label carbon, oxygen, and hydrogen atoms at different reaction sites.

The free-energy and electronic-energy potential energy surfaces (PESs) for the initiation reactions of OH radicals with HOCH₂OOH, HOCH(CH₃)OOH, and HOC(CH₃)₂OOH are presented in Figs. 2–4 and S1–S3 in the Supplement, respectively. The optimized geometries of all stationary points are displayed in Figs. S6–S8 in the Supplement, respectively. As can be seen in Fig. 2, the reaction of HOCH₂OOH with OH radicals proceeds through four pathways: H-abstraction from the -O₁H₁ (R1), -C₁H₃ (R2), -C₁H₄ (R3), and -O₂O₃H₂ (R4) groups. For each pathway, a pre-reactive complex with a six- or seven-membered ring structure is formed in the entrance channel, which is stabilized by hydrogen bond interactions between the oxygen atom of an OH radical and the abstraction hydrogen atom of HOCH₂OOH, and between the remnant hydrogen atom of an OH radical and one of the oxygen atoms of HOCH₂OOH (Fig. S6). Then, it surmounts the modest barrier that is higher in energy than the reactants to react. The reaction barriers ΔG_a^\ddagger decrease in the order of 6.4 (R1) > 5.8 (R2) \approx 5.4 (R3) > 1.5 (R4) kcal mol⁻¹, indicating that H-abstraction from the -O₂O₃H₂ group (R4) is more preferable than those from the -O₁H₁, -C₁H₃ and -C₁H₄ groups (R1–R3). The same conclusion is also derived from the energy barriers ΔE_a^\ddagger that R4 is the most favorable H-abstraction pathway (Fig. S1). The difference in barrier heights can be attributed to the bond dissociation energy (BDE) of the multiple types of bonds in the HOCH₂OOH molecule. BDE decreases in the order of 103.7 (O₁–H₁) > 98.2 (C₁–H₃) \approx 97.4 (C₁–H₄) > 87.2 (O₃–H₂) kcal mol⁻¹, and this order is consistent with that of the barrier heights of H-abstraction reactions. Their reaction free-energy values indicate that the exothermicity of R4 is the largest among these four H-abstraction reactions. Based on the above discussions, it is concluded that H-abstraction from the -O₂O₃H₂ group resulting in the formation of an HOCH₂OO radical (R4) is feasible both thermodynamically and kinetically.

Given the multiple reaction sites of hydrogen atoms, the atmospheric transformation of HOCH(CH₃)OOH from the *anti*-CH₃CHOO + H₂O reaction should have six possible H-abstraction pathways as presented in Fig. 3. As shown in

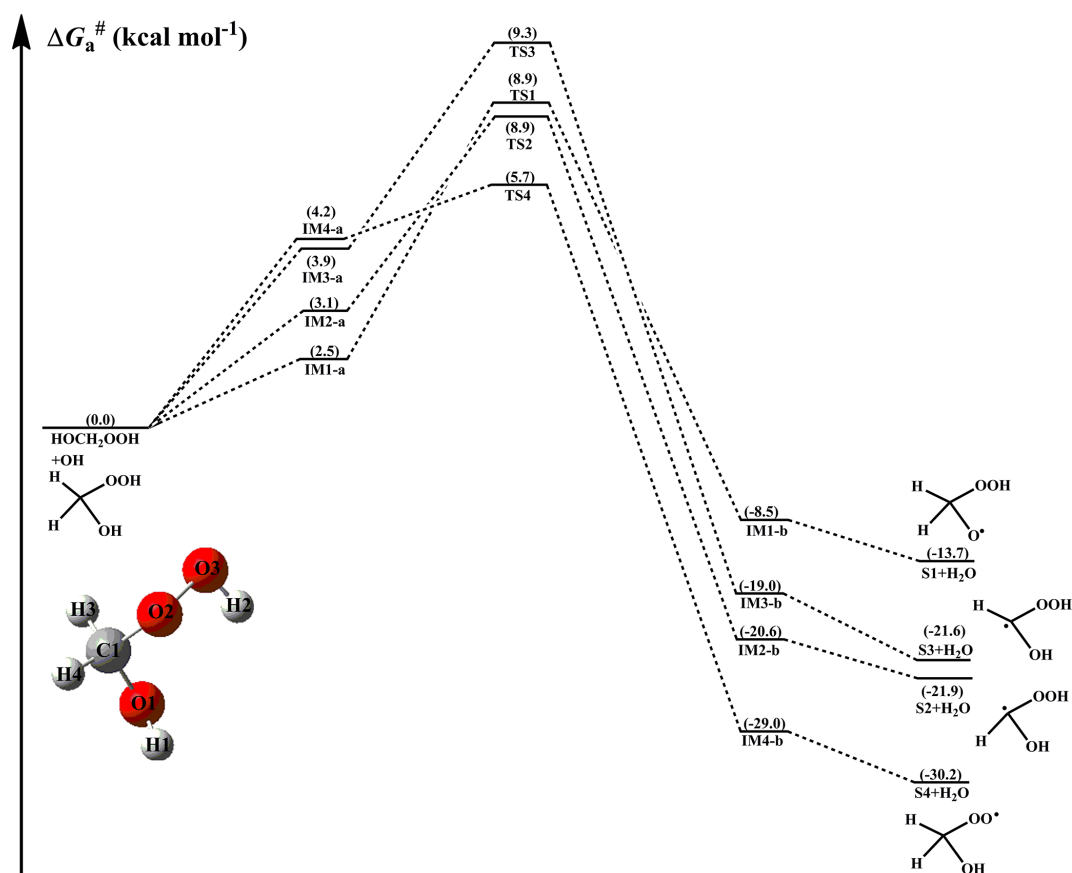


Figure 2. PES (ΔG_a^\ddagger) for the OH-initiated reactions of HOCH_2OOH from the $\text{CH}_2\text{OO} + \text{H}_2\text{O}$ reaction predicted at the M06-2X/ma-TZVP//M06-2X/6-311+G(2df,2p) level of theory (a and b represent the pre-reactive and post-reactive complexes).

Fig. 3, each H-abstraction reaction begins with the formation of a weakly bound hydrogen bonded pre-reactive complex with a six- or seven-membered ring structure in the entrance channel (Fig. S7). Then it immediately transforms into the respective product via the corresponding transition state. The ΔG_a^\ddagger of H-abstraction from the $-\text{C}_1\text{H}_3$ (R6) and $-\text{O}_2\text{O}_3\text{H}_2$ (R8) groups are 2.2 and 1.7 kcal mol^{-1} , respectively, which are $\sim 4\text{--}5 \text{ kcal mol}^{-1}$ lower than those from the $-\text{O}_1\text{H}_1$ (R5) and $-\text{CH}_3$ (R7) groups. This result shows that R6 and R8 have nearly identical importance in the atmosphere. Compared with the barriers of H-abstraction at the C_α -position (R6) and C_β -position (R7), it can be found that the former case is more favourable than the latter case. This conclusion is further supported by the Jara-Toro (2017, 2018) studies regarding the reactions of an OH radical with linear saturated alcohols (methanol, ethanol, and n-propanol) that H-abstraction at the C_α -position is predominant.

For the OH-initiated oxidation of $\text{HOCH}(\text{CH}_3)\text{OOH}$ from the $\text{syn-CH}_3\text{CHOO} + \text{H}_2\text{O}$ reaction, the corresponding free-energy and electronic-energy PESs are displayed in Figs. S4 and S5 in the Supplement, respectively. From Fig. S4, it can be seen that H-abstraction by OH radicals from $\text{HOCH}(\text{CH}_3)\text{OOH}$ has six possible pathways. For each path-

way, a pre-reactive complex is formed prior to the corresponding transition state, and then it overcomes a modest barrier to reaction. The ΔG_a^\ddagger of R6' and R8' are 2.3 and 1.8 kcal mol^{-1} , respectively, which are about 5 kcal mol^{-1} lower than those of R5' and R7'. The result shows that H-abstraction from the $-\text{CH}$ (R6') and $-\text{OOH}$ (R8') groups is preferable kinetically. The same conclusion is also derived from the energy barriers ΔE_a^\ddagger : the R6' and R8' are the most favourable H-abstraction pathways (Fig. S5). It should be noted that although the barriers of R6' and R8' are comparable, the exoergicity of R6' is significantly lower than that of R8'. The aforementioned conclusions are consistent with the results derived from the OH-initiated oxidation of $\text{HOCH}(\text{CH}_3)\text{OOH}$ from the *anti*- $\text{CH}_3\text{CHOO} + \text{H}_2\text{O}$ reaction. Zhou et al. (2019) demonstrated that the bimolecular reaction of *syn*- CH_3CHOO with water leading to the formation of $\text{HOCH}(\text{CH}_3)\text{OOH}$ is of less importance in the atmosphere, while the unimolecular decay to OH radicals is the major loss process of *syn*- CH_3CHOO . Therefore, in the present study, we mainly focus on the subsequent mechanism of intermediates generated from OH-initiated oxidation of $\text{HOCH}(\text{CH}_3)\text{OOH}$ from the *anti*- $\text{CH}_3\text{CHOO} + \text{H}_2\text{O}$ reaction.

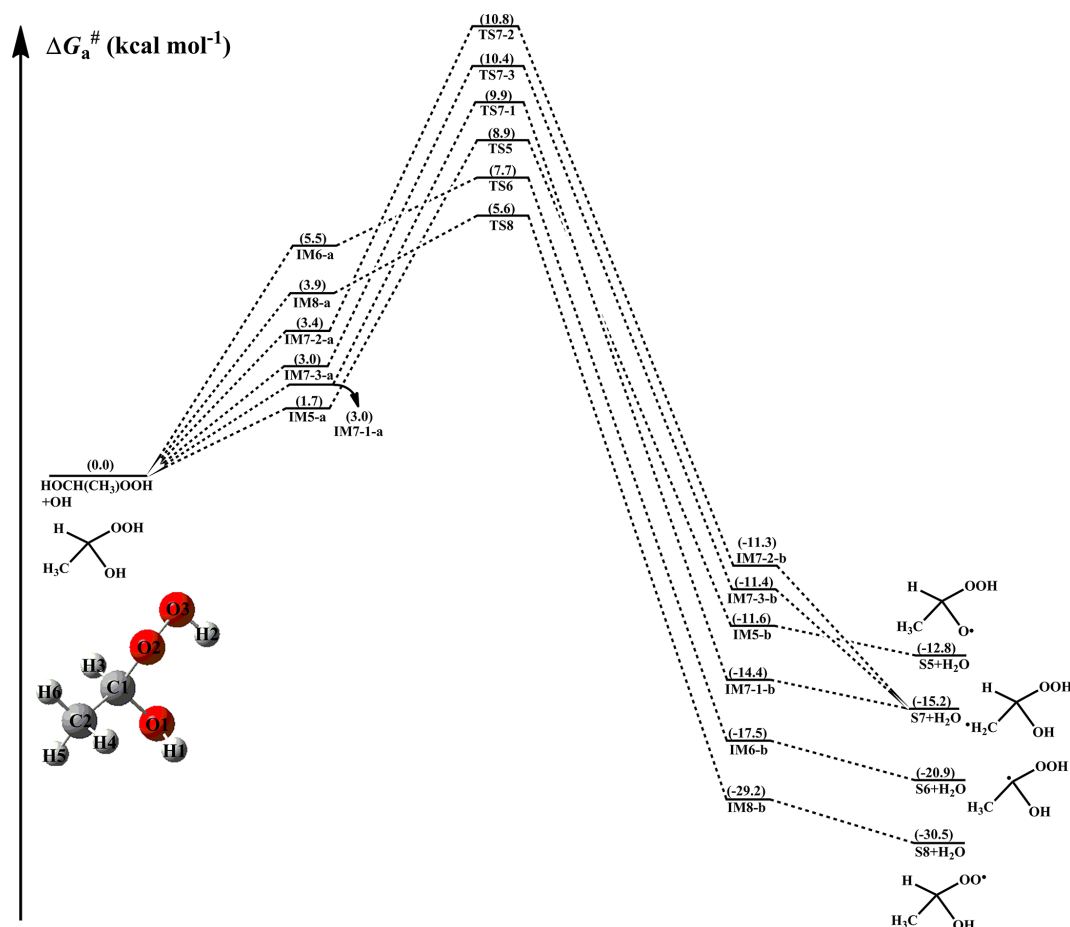


Figure 3. PES ($\Delta G_a^\#$) for the OH-initiated reactions of HOCH(CH₃)OOH from the *anti*-CH₃CHOO + H₂O reaction predicted at the M06-2X/ma-TZVP//M06-2X/6-311+G(2df,2p) level of theory (a and b represent the pre-reactive and post-reactive complexes).

From Fig. 4, it can be seen that H-abstraction from HOC(CH₃)₂OOH has eight possible H-abstraction pathways. All the H-abstraction reactions are strongly exothermic and spontaneous, suggesting that they are thermodynamically feasible under atmospheric conditions. It deserves mentioning that the release of energy of R12 is significantly greater than that of R9–R11. For each H-abstraction pathway, an RC with a six- or seven-membered ring structure is formed prior to the corresponding TS, which is more stable than the separate reactants due to the hydrogen bond interactions between HOC(CH₃)₂OOH and the OH radical. Then, the RC overcomes a modest barrier to reaction. The $\Delta G_a^\#$ of H-abstraction from the -O₂O₃H₂ group (R12) is 2.7 kcal mol⁻¹, which is the lowest among these eight H-abstraction reactions. This result again shows that H-abstraction from the -O₂O₃H₂ group is the dominant pathway.

The rate coefficients of each H-abstraction pathway involved in the initiation reactions of distinct HHPs with OH radicals are estimated over the temperature range from 273 to 400 K, as summarized in Tables S2–S4 and Figs. S9–

S11 in the Supplement. As shown in Table S2, the total rate coefficients k_{tot} of HOCH₂OOH reaction with OH radicals decrease slightly with increasing temperature. At ambient temperature, k_{tot} is estimated to be 3.3×10^{-11} cm³ molecule⁻¹ s⁻¹, which is a factor of ~ 5 greater than that ($(7.1 \pm 1.5) \times 10^{-12}$ cm³ molecule⁻¹ s⁻¹, at 295 K) reported by Allen et al. (2018), who derived the result from the reaction of HMHP with OH radicals through CF₃O⁻ chemical ionization mass spectrometry (CIMS) and laser-induced fluorescence (LIF). This discrepancy can be attributed to the uncertainties associated with the barrier height and tunneling correction. $k_{\text{R4(O3-H2)}}$ is 1 to 2 orders of magnitude greater than $k_{\text{R1(O1-H1)}}$, $k_{\text{R2(C1-H3)}}$, and $k_{\text{R3(C1-H4)}}$ in the whole temperature range, indicating that R4 is the most favorable H-abstraction pathway. For example, $k_{\text{R4(O3-H2)}}$ is calculated to be 2.9×10^{-11} cm³ molecule⁻¹ s⁻¹ at 298 K, which is higher than $k_{\text{R1(O1-H1)}}$ (1.8×10^{-13}), $k_{\text{R2(C1-H3)}}$ (9.9×10^{-13}), and $k_{\text{R3(C1-H4)}}$ (2.0×10^{-12}) by 161, 29, and 15 times, respectively.

From Table S3, it can be seen that the total rate coefficients k'_{tot} of the HOCH(CH₃)OOH reaction with OH rad-

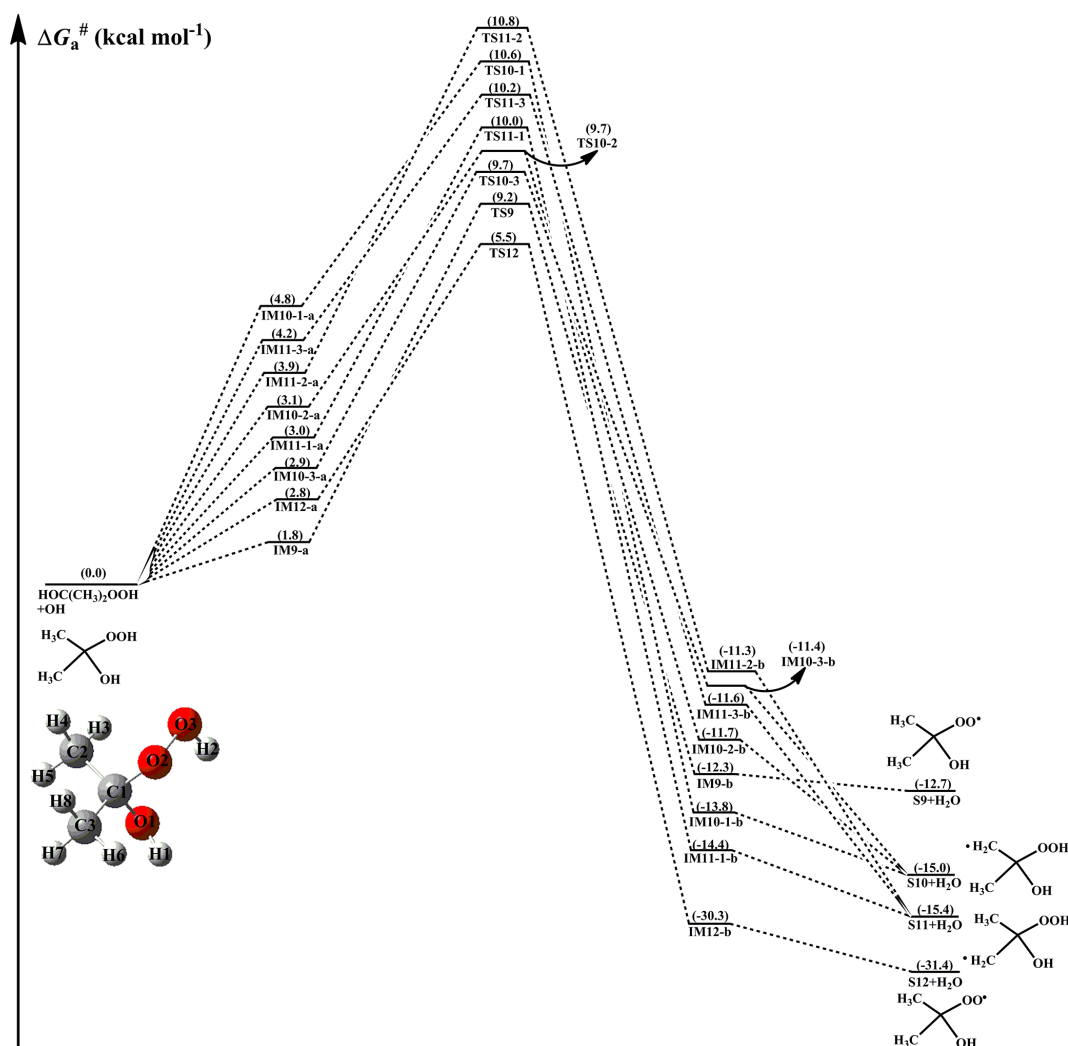


Figure 4. PES (ΔG_a^\ddagger) for the OH-initiated reactions of $\text{HOC}(\text{CH}_3)_2\text{OOH}$ from the $(\text{CH}_3)_2\text{COO} + \text{H}_2\text{O}$ reaction predicted at the M06-2X/ma-TZVP//M06-2X/6-311+G(2df,2p) level of theory (a and b represent the pre-reactive and post-reactive complexes).

icals decrease in the range between 4.5×10^{-11} (273 K) and 8.1×10^{-12} (400 K) $\text{cm}^3 \text{molecule}^{-1} \text{s}^{-1}$ with increasing temperature, and they exhibit a slightly negative temperature dependence. $k_{\text{R8}(\text{O3-H2})}$ is approximately identical to k'_{tot} in the full temperature range, and it is greater than $k_{\text{R5}(\text{O1-H1})}$, $k_{\text{R6}(\text{C1-H3})}$, $k_{\text{R7-1}(\text{C2-H4})}$, $k_{\text{R7-2}(\text{C2-H5})}$, and $k_{\text{R7-3}(\text{C2-H6})}$ by 1 to 2 orders of magnitude. The result also demonstrates in that H-abstraction from the -OOH group (R8) is preferable kinetically. It should be noted that although the barriers of R8 and R6 are comparable, $k_{\text{R8}(\text{O3-H2})}$ is greater than $k_{\text{R6}(\text{C1-H3})}$ by approximately 1 order of magnitude over the temperature range studied. The most likely reason is the stability of pre-reactive complexes that IM8-a is more stable than IM6-a in energy. A similar conclusion is derived from the rate coefficients of the $\text{HOC}(\text{CH}_3)_2\text{OOH} + \text{OH}$ reaction in that H-abstraction from the -OOH group (R12) is favorable kinetically (Table S4). The atmospheric lifetimes of HOCH_2OOH ,

$\text{HOCH}(\text{CH}_3)\text{OOH}$, and $\text{HOC}(\text{CH}_3)_2\text{OOH}$ reactivity toward OH radicals are estimated to be 0.58–1.74, 0.60–1.79, and 1.23–3.69 h, respectively, at room temperature under typical OH radical concentrations of $5\text{--}15 \times 10^6 \text{ molecules cm}^{-3}$ during daylight (Long et al., 2017).

In summary, the dominant pathway is H-abstraction from the -OOH group in the initiation reactions of OH radicals with HOCH_2OOH . H-abstraction from the -CH group is competitive with that from the -OOH group in the reaction of OH radicals with $\text{HOCH}(\text{CH}_3)\text{OOH}$. Compared with the barriers of H-abstraction from the -OOH and -CH₂ groups in the reaction of OH radicals with HOCH_2OOH , the barrier of H-abstraction from the -CH group is reduced by $3.6 \text{ kcal mol}^{-1}$, whereas the barrier of H-abstraction from the -OOH group is increased by $0.2 \text{ kcal mol}^{-1}$ when a methyl group substitution occurs at the C₁-position of HOCH_2OOH . The dominant pathway is H-abstraction from the -OOH group in the

reaction of OH radicals with $\text{HOC}(\text{CH}_3)_2\text{OOH}$, and its barrier height is increased by 1.2 kcal mol^{-1} compared with the $\text{OH} + \text{HOCH}_2\text{OOH}$ system. The barrier of H-abstraction from the -OOH group slightly increases when the number of methyl groups increases. It is interesting to compare the rate coefficient of the dominant pathway in the $\text{OH} + \text{HOCH}_2\text{OOH}$ system with those of the analogous reactions in the $\text{OH} + \text{HOCH}(\text{CH}_3)\text{OOH}$ and $\text{OH} + \text{HOC}(\text{CH}_3)_2\text{OOH}$ reactions. It can be found that the rate coefficient is almost identical when a methyl group substitution occurs at the C_1 -position, whereas the rate coefficient decreases by a factor of 2–5 when two methyl groups are introduced at the C_1 -position.

3.2 Subsequent reactions of H-abstraction products of RO_2 radicals in pristine environments

In principle, the H-abstraction products of RO_2 radicals have three possible fates in pristine environments: (1) the self-reactions of RO_2 radicals can produce $\text{RO} + \text{R}'\text{O} + \text{O}_2$ (propagation channel), or generate $\text{ROH} + \text{R}'(-\text{H}, =\text{O}) + \text{O}_2$ or produce $\text{ROOR} + \text{O}_2$ (termination channel), which is recognized as an important SOA precursor (Berndt et al., 2018; Zhang et al., 2012); (2) the RO_2 radicals react with HO_2 radicals to form hydroperoxide ROOH , alcohol, OH, and other products (Winiberg et al., 2016; Chen et al., 2021); (3) the RO_2 radicals undergo autoxidation through intramolecular H-shift and alternating O_2 -addition steps to generate HOMs (Ehn et al., 2014; Bianchi et al., 2019; Nozière and Vereecken, 2019; Rissanen et al., 2014). The three aforementioned reactions are discussed in further detail in the subsequent subsections.

3.2.1 Reaction mechanism for the self-reaction of RO_2 radicals

Self-reaction is a dominant removal pathway for RO_2 radicals under low concentrations of NO and high concentrations of RO_2 radicals. The self-reaction of RO_2 radicals usually follows the Russell mechanism (Russell, 1957), and has four main possible pathways: (1) $2\text{RO}_2 \rightarrow 2\text{RO} + \text{O}_2$; (2) $2\text{RO}_2 \rightarrow \text{ROH} + \text{R}'\text{CO} + \text{O}_2$; (3) $2\text{RO}_2 \rightarrow \text{ROOR} + \text{O}_2$; and (4) $2\text{RO}_2 \rightarrow \text{ROOH} + \text{R}'\text{CHOO}$ (Atkinson and Arey, 2003). The relative importance of different pathways varies considerably depending on the nature of RO_2 radicals (Valiev et al., 2019; Lee et al., 2016). A schematic PES for the self-reaction of HOCH_2OO radicals is drawn in Fig. 5. As can be seen in Fig. 5, the self-reaction of HOCH_2OO radicals starts with the formation of tetroxide complexes IM13-a and IM14-a in the entrance channel, with 2.9 and 3.4 kcal mol^{-1} stability. Then they fragment into dimer $\text{S13} + {}^1\text{O}_2$ (R13) and $\text{HOCH}_2\text{OOH} + \text{HOCHOO}$ (R14) via TS13 and TS14 with the barriers of 43.3 and $51.5\text{ kcal mol}^{-1}$, respectively. However, the barriers of R13 and R14 are extremely high, making them irrelevant in the atmosphere.

From Fig. 5, it is seen that the self-reaction of HOCH_2OO radicals proceeds via oxygen-to-oxygen coupling leading to the formation of tetroxide intermediate S14 with the electronic-energy and free-energy barriers of 7.3 and $19.6\text{ kcal mol}^{-1}$. Kumar and Francisco reported an electronic-energy barrier of $14.0\text{ kcal mol}^{-1}$ for the gas-phase decomposition of the HOCH_2OO radical, which may be a new source of HO_2 radicals in the troposphere (Kumar and Francisco, 2015, 2016). Compared with the electronic-energy barriers of the unimolecular dissociation of the HOCH_2OO radical and its self-reaction, it can be found that the self-reaction of the HOCH_2OO radical resulting in the formation of S14 is significantly feasible. The formed S14 can fragment into $\text{HOCH}_2\text{O} + \text{HCOOH} + \text{HO}_2$ via a concerted process of $\text{O}_2\text{--O}_3$ and $\text{O}_5\text{--O}_6$ bond rupture and $\text{O}_3\text{--H}_6$ bond formation with a barrier of $29.8\text{ kcal mol}^{-1}$. Alternatively, S14 can convert into the caged tetroxide intermediate S16 through asymmetric two-step $\text{O}_2\text{--O}_3$ and $\text{O}_5\text{--O}_6$ bond scission with the barriers of 19.1 and 3.1 kcal mol^{-1} , respectively. The result shows that the latter pathway is preferred over the former channel owing to its lower barrier. The overall spin multiplicity of S16 is singlet, in which the O_2 moiety maintains the triplet ground state (spin up) and is very loosely bound. In order to preserve overall singlet multiplicity, the two HOCH_2O radical pairs (${}^3(\text{HOCH}_2\text{O} \cdots \text{HOCH}_2\text{O})$) must have triplet multiplicity (spin down). S16 can be regarded as the ground state ${}^3\text{O}_2$ moving away from the two HOCH_2O radical pairs that keep interacting. Due to the difficulty in performing the constrained optimization for the dissociation of S16, the ${}^3\text{O}_2$ moiety is considered as a leaving moiety away from two HOCH_2O radical pairs, and merely the dissociation of ${}^3(\text{HOCH}_2\text{O} \cdots \text{HOCH}_2\text{O})$ is taken into consideration in the present study. It has three types of pathways: (1) it yields HOCH_2OH and excited-state ${}^3\text{HCOOH}$ through an alpha hydrogen transfer with a barrier of 14.0 and $10.2\text{ kcal mol}^{-1}$ exothermicity, followed by the excited ${}^3\text{HCOOH}$ to go back to the ground-state ${}^1\text{HCOOH}$; (2) it generates two HOCH_2O radicals via a barrierless process with an exoergicity of $16.9\text{ kcal mol}^{-1}$; (3) it produces dimer S17 via an intersystem crossing (ISC) step with an exoergicity of $32.1\text{ kcal mol}^{-1}$. Based on the calculated reaction barriers, the rate-limiting step is the cleavage of the $\text{O}_2\text{--O}_3$ bond (R17) in the unimolecular decay processes of S14. This conclusion coincides with the previous result obtained from the dissociation of di-*t*-butyl tetroxide that the rate-controlling step is the rupturing of a single O–O bond (Lee et al., 2016). Valiev et al. (2019) proposed that the ISC rate of the ROOR dimer formed from various $(\text{RO} \cdots \text{R}'\text{O})$ systems is extremely high ($> 10^8\text{ s}^{-1}$) and exhibits a strong stereoselectivity.

Figure 6 depicts a schematic PES for the self-reaction of the $\text{HOCH}(\text{CH}_3)\text{OO}$ radical. As shown in Fig. 6, the self-reaction of the $\text{HOCH}(\text{CH}_3)\text{OO}$ radical can produce either dimer S18 and ${}^1\text{O}_2$ via TS20 with a barrier of $44.4\text{ kcal mol}^{-1}$, or $\text{HOCH}(\text{CH}_3)\text{OOH}$ and $\text{HOC}(\text{CH}_3)\text{OO}$ through TS21 with a barrier of $54.3\text{ kcal mol}^{-1}$. But the

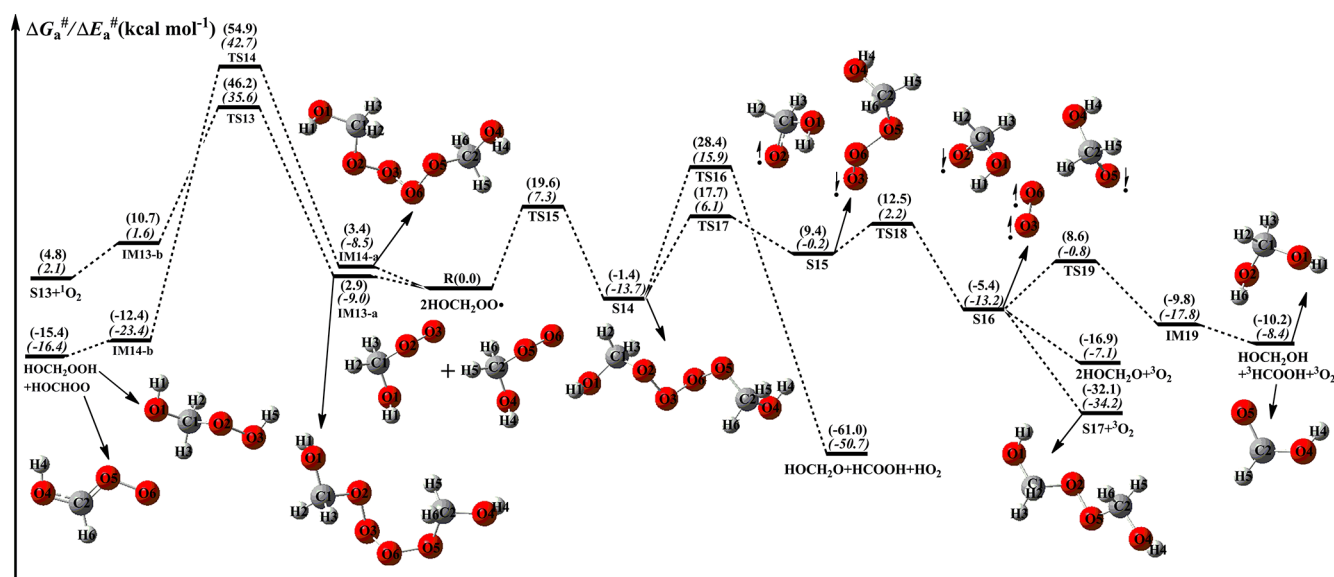


Figure 5. PES (ΔG_a^\ddagger and ΔE_a^\ddagger in italics) for the self-reaction of HOCH_2OO radicals predicted at the M06-2X/ma-TZVP//M06-2X/6-311+G(2df,2p) level of theory.

barriers of R20 and R21 are considerably high, making them of less importance in the atmosphere. Alternatively, the self-reaction of the $\text{HOCH}(\text{CH}_3)\text{OO}$ radical proceeds via oxygen-to-oxygen coupling to form the tetroxide intermediate S19 with a barrier of $19.9 \text{ kcal mol}^{-1}$ (Fig. 6). The formed S19 proceeds through asymmetric two-step $\text{O}_2\text{--O}_3$ and $\text{O}_5\text{--O}_6$ bond scission to produce the caged tetroxide intermediate S21 of overall singlet multiplicity comprising two same-spin alkoxy radicals (spin down) and triplet oxygen (spin up). These two processes overcome the barriers of 21.4 and $1.3 \text{ kcal mol}^{-1}$. Then, S21 decomposes into the propagation ($2\text{HOCH}(\text{CH}_3)\text{O} + {}^3\text{O}_2$) and termination products ($\text{HOCH}(\text{CH}_3)\text{OH} + {}^3\text{CH}_3\text{OOH} + {}^3\text{O}_2$ and dimer S22 + ${}^3\text{O}_2$) with an exoergicity of 12.5 , 11.7 , and $33.0 \text{ kcal mol}^{-1}$. The rate-determining step is the rupturing of $\text{O}_2\text{--O}_3$ bond (R24) in the dissociation processes of S19.

As shown in Fig. 7, the dominant pathway for the self-reaction of the $\text{HO}(\text{CH}_3)_2\text{COO}$ radical begins with the formation of tetroxide intermediate S24 via oxygen-to-oxygen coupling transition state TS28 with a barrier of $20.4 \text{ kcal mol}^{-1}$; then it transforms into the caged tetroxide intermediate S26 of overall singlet spin multiplicity through asymmetric two-step O--O bond cleavage with the barriers of 22.0 and $3.4 \text{ kcal mol}^{-1}$; finally, S26 can produce either two $\text{HO}(\text{CH}_3)_2\text{CO}$ radicals with an exoergicity of $10.3 \text{ kcal mol}^{-1}$, or dimer S27 with an exoergicity of $31.5 \text{ kcal mol}^{-1}$. Compared with the self-reactions of HOCH_2OO and $\text{HOCH}(\text{CH}_3)\text{OO}$ radicals, the termination product of the self-reaction of the $\text{HOC}(\text{CH}_3)_2\text{OO}$ radical is exclusively dimer S27 because of the absence of an alpha hydrogen atom in the latter. Compared with the barrier of the rate-determining route R17 in the self-reaction of the

HOCH_2OO radical, the barrier of the rate-limiting step R29 is increased by about $3.0 \text{ kcal mol}^{-1}$ when two methyl substitutions are introduced at the C_1 -position of the HOCH_2OO radical. The reason might be attributed to the cage escape of alkoxy radicals. Therefore, tertiary RO_2 radicals have great opportunities to react with the HO_2 radical or undergo autoxidation in pristine environments.

3.2.2 Reaction mechanism for the reaction of RO_2 radicals with an HO_2 radical

When NO is present in low concentrations, the bimolecular reaction of RO_2 radicals with the HO_2 radical is generally expected to be the dominant pathway. The primary sources of HO_2 radicals include the photo-oxidation of oxygenated volatile organic compounds (OVOCs) and the ozonolysis reaction, as well as the secondary sources include the reactions of the OH radical with CO, ozone, and VOCs, the reaction of the alkoxy radical RO with O_2 , and the red-light-induced decomposition of the α -hydroxy methylperoxy radical OHCH_2OO (Kumar and Francisco, 2015; Stone et al., 2012; Hofzumahaus et al., 2009). The atmospheric concentration of HO_2 radicals is $1.5\text{--}10 \times 10^8 \text{ molecules cm}^{-3}$ at the ground level in polluted urban environments (Stone et al., 2012). A schematic PES for the reactions of distinct RO_2 radicals with HO_2 the radical is presented in Fig. 8. As shown in Fig. 8, all the reactions are strongly exothermic and spontaneous, indicating that they are thermodynamically feasible in the atmosphere. The reaction of HOCH_2OO with HO_2 (R31) starts with the formation of a pre-reactive complex IM31-a in the entrance channel, which is more stable than the separate reactants by $3.8 \text{ kcal mol}^{-1}$. Then, IM31-a converts into

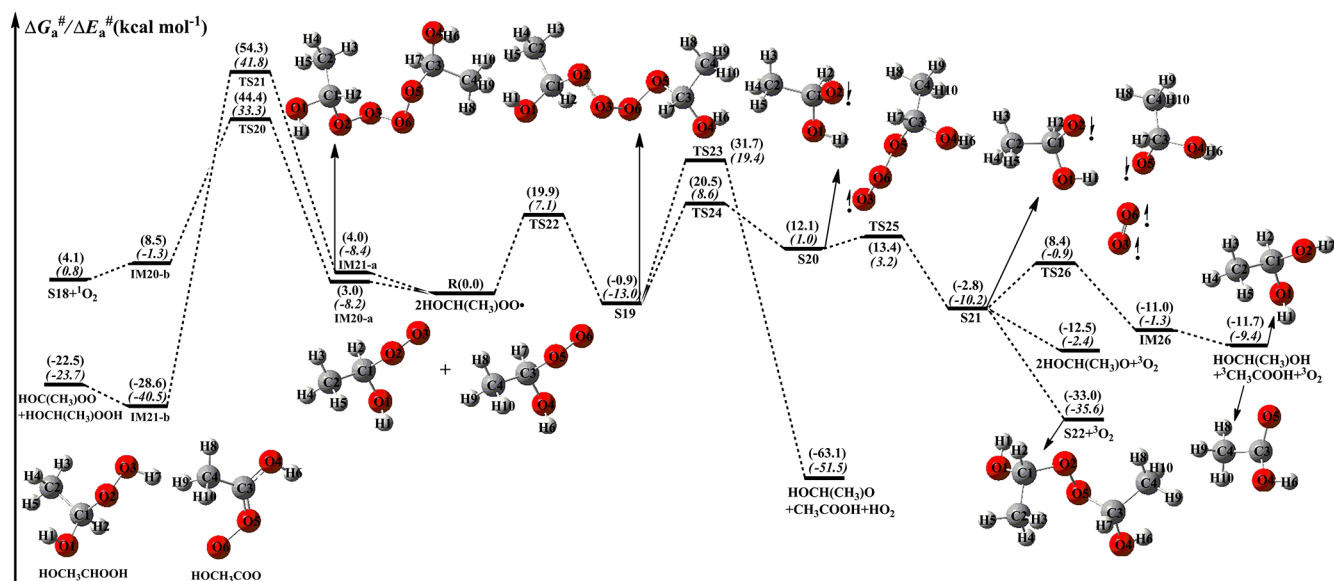


Figure 6. PES ($\Delta G_a^\#$ and $\Delta E_a^\#$, in italics) for the self-reaction of $\text{HOCH}(\text{CH}_3)\text{OO}$ radicals predicted at the M06-2X/ma-TZVP//M06-2X/6-311+G(2df,2p) level of theory.

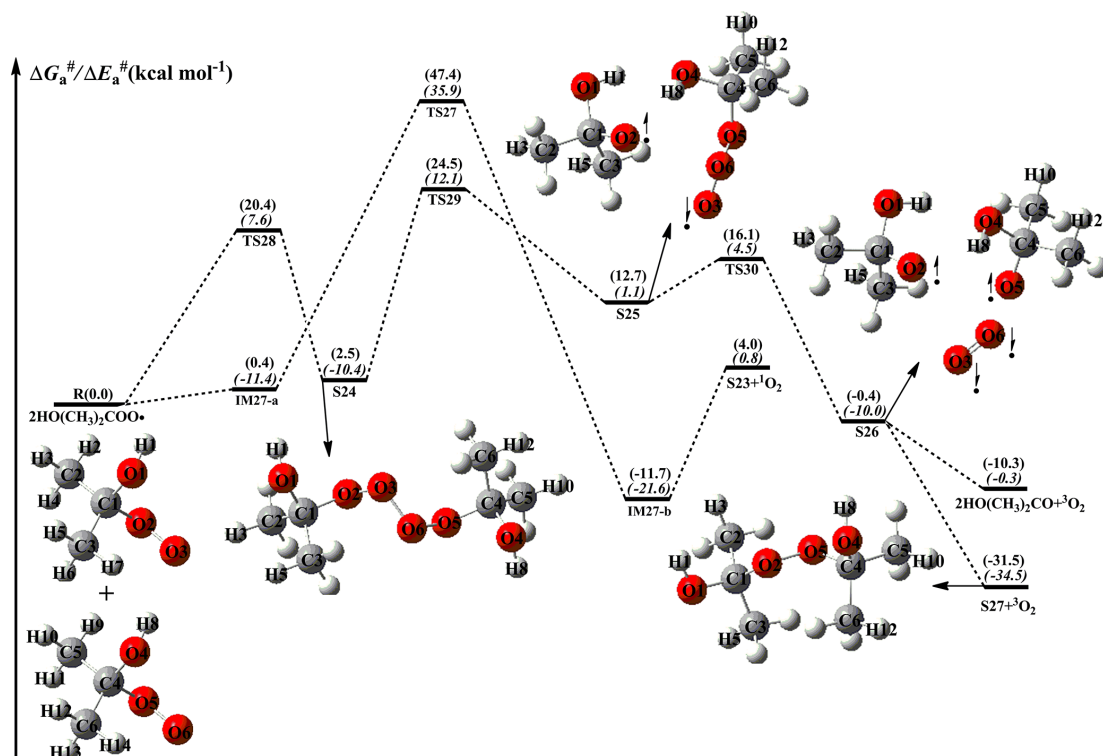


Figure 7. PES ($\Delta G_a^\#$ and $\Delta E_a^\#$, in italics) for the self-reaction of $\text{HO}(\text{CH}_3)_2\text{COO}$ radicals predicted at the M06-2X/ma-TZVP//M06-2X/6-311+G(2df,2p) level of theory.

HOCH_2OOH and O_2 via a hydrogen atom transfer from the HO_2 radical to the terminal oxygen atom of the HOCH_2OO radical with a barrier of $2.0 \text{ kcal mol}^{-1}$. The mechanisms of $\text{HOCH}(\text{CH}_3)\text{OO} + \text{HO}_2$ (R32) and $\text{HO}(\text{CH}_3)_2\text{COO} + \text{HO}_2$ (R33) reactions are similar to that of the $\text{HOCH}_2\text{OO} + \text{HO}_2$ system. In order to avoid redundancy, a detailed discussion of the aforementioned mechanisms is not provided in the present study. Compared with the barrier of the $\text{HOCH}_2\text{OO} + \text{HO}_2$ reaction, the barrier height is lower by only $0.1 \text{ kcal mol}^{-1}$ when one or two methyl substitutions occur at the C_1 -position of the HOCH_2OO radical. This result suggests that the barrier height is not influenced by the number of methyl substitutions. The rate coefficients of the reactions of distinct RO_2 radicals with the HO_2 radical are summarized in Table S5 and Fig. S12 in the Supplement. As shown in Table S5, the rate coefficients k_{R31} of the $\text{HOCH}_2\text{OO} + \text{HO}_2$ reaction vary from 3.1×10^{-11} (273 K) to $2.1 \times 10^{-12} \text{ cm}^3 \text{ molecule}^{-1} \text{ s}^{-1}$ (400 K), and they exhibit a negative temperature dependence. A similar conclusion is also obtained from the rate coefficients k_{R32} and k_{R33} in that they decrease with the temperature increasing. Notably, the rate coefficient slightly increases when the number of methyl groups increases. At ambient temperature, k_{R31} is estimated to be $1.7 \times 10^{-11} \text{ cm}^3 \text{ molecule}^{-1} \text{ s}^{-1}$, which is consistent with the value of $\sim 2 \times 10^{-11} \text{ cm}^3 \text{ molecule}^{-1} \text{ s}^{-1}$ for the reaction of acyl peroxy radicals with the HO_2 radical (Wennberg et al., 2018). The typical atmospheric concentrations of HO_2 radicals are 5, 20, and 50 pptv in urban, rural, and forest environments, respectively (Bianchi et al., 2019), which translate into the pseudo-first-order rate constants $k'_{\text{HO}_2} = k_{\text{HO}_2}[\text{HO}_2]$ of 1.1×10^{-3} , 4.2×10^{-3} and $1.1 \times 10^{-2} \text{ s}^{-1}$, respectively.

3.2.3 Reaction mechanism for the isomerization of RO_2 radicals

The autoxidation of RO_2 radicals is known to play an important role in the (re)generation of HO_x radicals and the formation of HOMs (Xu et al., 2014; Bianchi et al., 2019; Rissanen et al., 2014; Ehn et al., 2017). The autoxidation mechanism includes an intramolecular H-shift from the $-\text{CH}_3$ or $-\text{CH}_2-$ groups to the $-\text{OO}$ site, leading to the formation of a hydroperoxyalkyl radical QOOH , followed by O_2 -addition to form a new peroxy radical (HOOQO_2), one after the other, resulting in the formation of HOMs (Rissanen et al., 2014; Berndt et al., 2015). For the H-shift reactions of RO_2 radicals, reactants, transition states and products have multiple conformers due to the effect of the degree of freedom for internal rotation. The calculated results show that the HOCH_2OO radical has four energetically similar conformers ($\text{HOCH}_2\text{OO-a}$, $\text{HOCH}_2\text{OO-b}$, $\text{HOCH}_2\text{OO-c}$, and $\text{HOCH}_2\text{OO-d}$). The relative free energy and Boltzmann population (w_i) of each individual conformer are listed in Table S6 in the Supplement, which indicate that the Boltzmann

populations of these four conformers are 46.39 %, 46.31 %, 2.99 %, and 4.32 %, respectively.

A schematic PES for the H-shift reaction of an HOCH_2OO radical is displayed in Fig. 9. As can be seen in Fig. 9, the lowest-energy conformer $\text{HOCH}_2\text{OO-a}$ can proceed via a 1,3-H shift from the $-\text{CH}_2$ group to the terminal oxygen leading to the formation of S28-a (HOCHOOH) with a barrier of $41.6 \text{ kcal mol}^{-1}$. $\text{HOCH}_2\text{OO-b}$ can isomerize to S28-b1 and S28-b2 via the four-membered ring transition states TS34-b1 and TS34-b2 (1,3-H shifts) with the barriers of 41.6 and $45.0 \text{ kcal mol}^{-1}$, respectively. However, the 1,3-H shift reactions have comparatively high barriers, making them irrelevant in the atmosphere. Despite many attempts, the transition states of the H-shift reactions of $\text{HOCH}_2\text{OO-c}$ and $\text{HOCH}_2\text{OO-d}$ could not be located. The result suggests that the H-shift reactions of these two conformers are inhibited, which is consistent with the previous study that not all reactants will be in a conformation with a path across the barrier to reaction in the H-shift reactions of RO_2 radicals (Møller et al., 2016). Similar to the case of the HOCH_2OO radical, the isomerization of the $\text{HOCH}(\text{CH}_3)\text{OO}$ radical proceeds via the 1,3- and 1,4-H shifts from the $-\text{CH}$ or $-\text{CH}_3$ groups to the terminal oxygen, resulting in the formation of hydroperoxyalkyl radicals (Fig. S13 in the Supplement). These 1,3- and 1,4-H shift reactions are accompanied by extremely high barriers ($> 37.9 \text{ kcal mol}^{-1}$), indicating that they are of less importance in the atmosphere. A similar conclusion is also derived from the isomerization of the $\text{HO}(\text{CH}_3)_2\text{COO}$ radical in that 1,4-H shift reactions are unfavourable kinetically (Fig. S14 in the Supplement). The high barriers of the 1,3- and 1,4-H shifts can be interpreted as the result of the larger ring strain energy (RSE) in the cyclic transition state geometries. Consequently, the isomerization reactions of HOCH_2OO , $\text{HOCH}(\text{CH}_3)\text{OO}$, and $\text{HO}(\text{CH}_3)_2\text{COO}$ radicals are unlikely to proceed in the atmosphere. This conclusion is further supported by previous studies, which found that the intramolecular H-shift isomerizations are important only for RO_2 radicals with large carbon structures (Crounse et al., 2013; Jokinen et al., 2014; Rissanen et al., 2014).

The single-conformer rate coefficients ($k_{\text{IRC-TST}}$) and multi-conformer rate coefficients ($k_{\text{MC-TST}}$) of the isomerization of HOCH_2OO , $\text{HOCH}(\text{CH}_3)\text{OO}$, and $\text{HOC}(\text{CH}_3)_2\text{OO}$ radicals are calculated over the temperature range of 273–400 K as listed in Table S9–S11 in the Supplement. As can be seen in Table S9, $k_{\text{IRC-TST}}$ of each conformer exhibits a marked positive temperature dependence over the temperature range studied. $k_{\text{MC-TST}}$ increases significantly with rising temperature, suggesting that a temperature increase promotes the isomerization of the HOCH_2OO radical. A similar conclusion is also obtained for the isomerization of $\text{HOCH}(\text{CH}_3)\text{OO}$ and $\text{HOC}(\text{CH}_3)_2\text{OO}$ radicals (Tables S10–S11). Notably, $k_{\text{MC-TST}}$ increases rapidly when the number of methyl groups increases. For example, the room temperature $k_{\text{MC-TST}}$ of HOCH_2OO radical isomerization is calculated to be $4.4 \times 10^{-16} \text{ s}^{-1}$, which is lower than those of

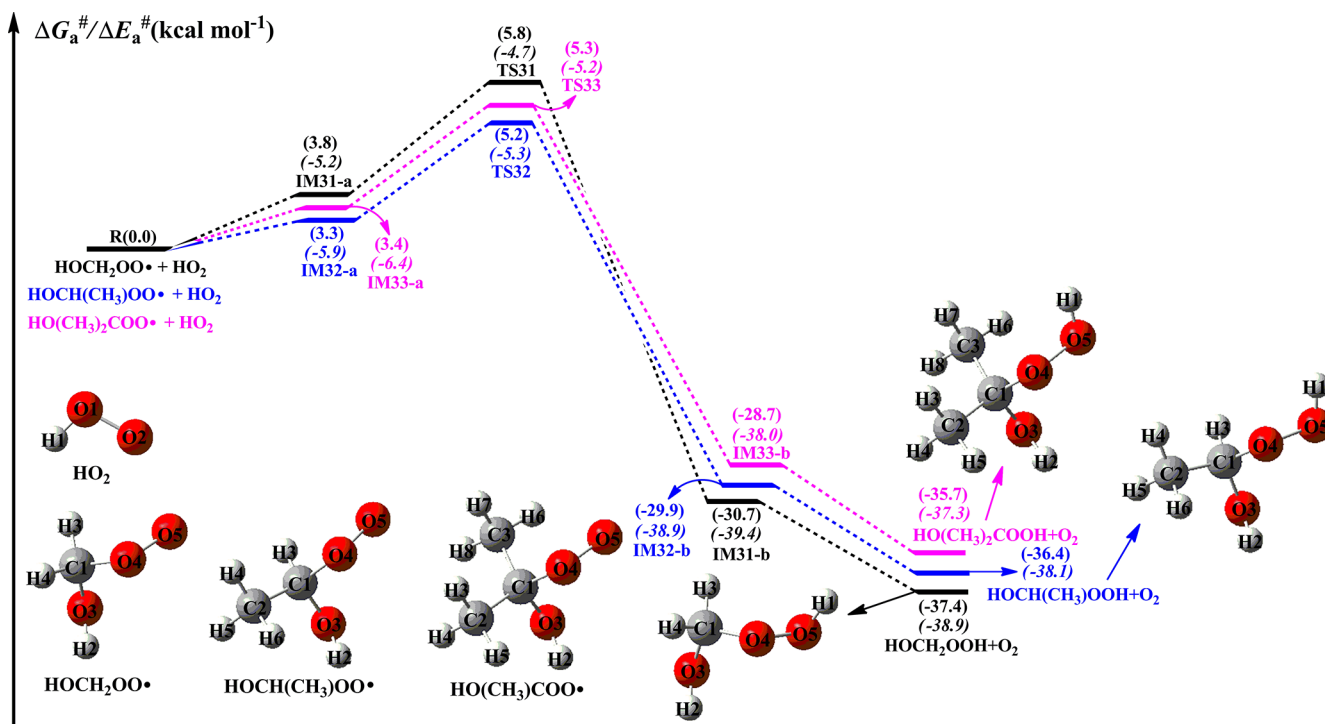


Figure 8. PES ($\Delta G_a^\#$ and $\Delta E_a^\#$, in italics) for the reactions of distinct RO₂ radicals with the HO₂ radical predicted at the M06-2X/ma-TZVP//M06-2X/6-311+G(2df,2p) level of theory.

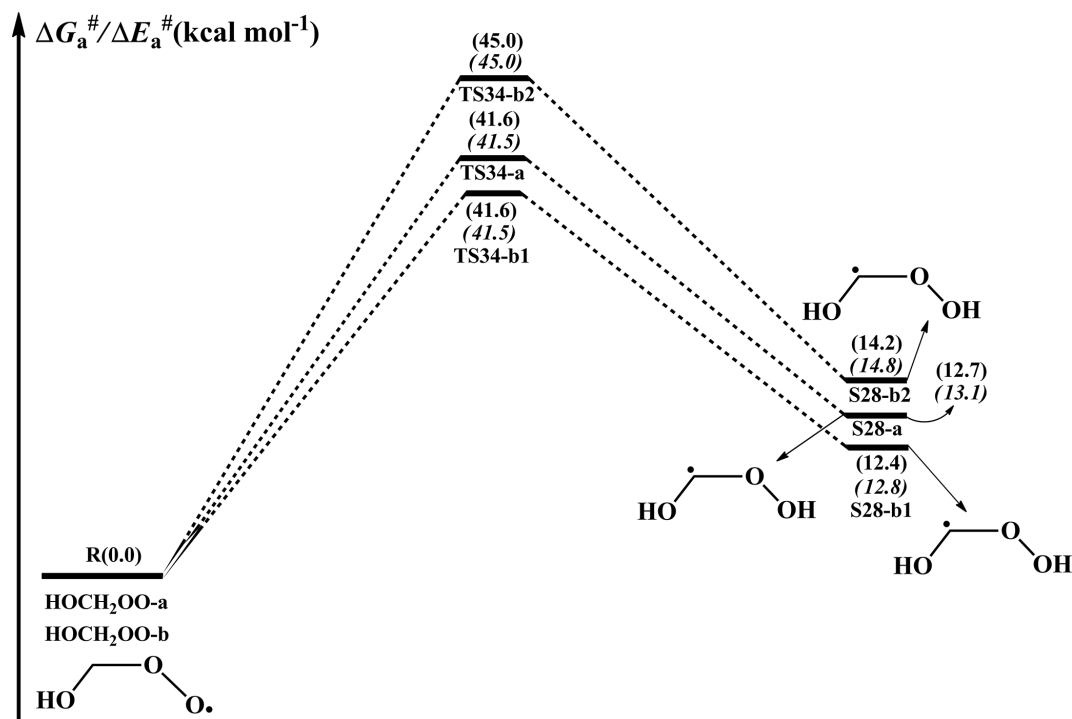


Figure 9. PES ($\Delta G_a^\#$ and $\Delta E_a^\#$, in italics) for the isomerization of an HOCH₂OO radical predicted at the M06-2X/ma-TZVP//M06-2X/6-311+G(2df,2p) level of theory.

the $\text{HOCH}(\text{CH}_3)\text{OO}$ ($2.9 \times 10^{-13} \text{ s}^{-1}$) and $\text{HO}(\text{CH}_3)_2\text{COO}$ ($3.0 \times 10^{-12} \text{ s}^{-1}$) radicals' isomerization by 660 and 6820 times, respectively.

3.3 Subsequent reactions of H-abstraction products of RO_2 radicals in urban environments

NO_x is present in high concentrations in urban environments, and reaction with NO is the dominant chemical sink for RO_2 radicals (Atkinson and Arey, 2003; Orlando and Tyndall, 2012; Perring et al., 2013). The main pathways for this type of reaction lead to the formation of NO_2 , RO radicals, organic nitrites, and organic nitrates at yields that are highly dependent on the nature of the R group (Orlando and Tyndall, 2012). The formation of NO_2 through subsequent photolysis ($\lambda < 420 \text{ nm}$) produces ozone and NO, increasing the concentrations of near-surface ozone and propagating the NO_x chain (Orlando and Tyndall, 2012). The schematic PES for the reactions of distinct RO_2 radicals with NO are displayed in Figs. 10–12. As shown in Fig. 10, the bimolecular reaction of an HOCH_2OO radical with NO initially leads to the formation of nitrite adduct S31 via the barrierless addition of NO to the terminal oxygen atom O_3 of the HOCH_2OO radical. The formed S31 exists as two isomers: S31-*cis* refers to O_2 and O_4 on the same side ($\text{DO}_2\text{O}_3\text{N}_1\text{O}_4 = 2.3^\circ$) with respect to the $\text{O}_3\text{--N}_1$ bond, whereas S31-*trans* refers to O_2 and O_4 on the opposite side ($\text{DO}_2\text{O}_3\text{N}_1\text{O}_4 = -179.8^\circ$) with respect to the $\text{O}_3\text{--N}_1$ bond. The calculations show that S31-*cis* is more stable than S31-*trans* by $1.1 \text{ kcal mol}^{-1}$ in energy. Tautomerization between S31-*cis* and S31-*trans* proceeds through the rotation of the $\text{O}_3\text{--N}_1$ bond with a barrier of $14.4 \text{ kcal mol}^{-1}$, implying that they can be regarded as separate atmospheric species. According to the Boltzmann-weighted distribution, the predicted proportions of S31-*cis* and S31-*trans* at room temperature are 86.5 % and 13.5 %, respectively. This result suggests that the dominant product of the reaction of an HOCH_2OO radical with NO is S31-*cis*, so it is selected as a model compound in order to gain insight into the mechanism of secondary reactions in the following sections.

S31-*cis* can either isomerize to organic nitrate S32 (R38) via a concerted process of $\text{O}_2\text{--O}_3$ bond breaking and $\text{O}_2\text{--N}_1$ bond formation with a barrier of $47.8 \text{ kcal mol}^{-1}$, or decompose into an HOCH_2O radical and NO_2 (R39) via the cleavage of the $\text{O}_2\text{--O}_3$ bond with a barrier of $11.3 \text{ kcal mol}^{-1}$. The result shows that the latter pathway is more favourable than the former channel. A similar conclusion is also obtained from the reactions of NO with $\text{HOCH}(\text{CH}_3)\text{OO}$ and $\text{HO}(\text{CH}_3)_2\text{COO}$ radicals in that the formation of organic nitrate is of minor importance in the atmosphere. This result is further supported by prior studies, which found that the direct formation of organic nitrate from peroxy nitrites is a minor channel for the reactions of isoprene-derived RO_2 radicals with NO (Piletic et al., 2017; Zhang et al., 2002). It should be noted that the transition state TS39 is not lo-

cated using the M06-2X functional, but it is located at the MP2/6-311+G(2df,2p) level of theory and is verified using IRC calculations. The HOCH_2O radical formed has two possible pathways: (1) it directly decomposes into CH_2O and an OH radical (R40) via β -site $\text{C}_1\text{--O}_1$ bond scission with a barrier of $52.4 \text{ kcal mol}^{-1}$; (2) it converts into HCOOH and an HO_2 radical (R41) through H-abstraction by O_2 with a barrier of $26.4 \text{ kcal mol}^{-1}$. This result reveals that R41 is the most feasible channel in the fragmentation of the HOCH_2O radical.

From Fig. 11, it can be seen that the addition of NO to an $\text{HOCH}(\text{CH}_3)\text{OO}$ radical leading to the formation of S33-*cis* is barrierless. Then, it decomposes into an $\text{HOCH}(\text{CH}_3)\text{O}$ radical and NO_2 (R44) via the cleavage of the $\text{O}_2\text{--O}_3$ bond with a barrier of $11.5 \text{ kcal mol}^{-1}$. The resulting $\text{HOCH}(\text{CH}_3)\text{O}$ radical has three possible pathways. The first is β -site $\text{C}_1\text{--C}_2$ bond scission leading to the formation of $\text{HCOOH} + \text{CH}_3$ (R45) with a barrier of $8.3 \text{ kcal mol}^{-1}$. The second is β -site $\text{C}_1\text{--O}_1$ bond cleavage resulting in the formation of $\text{CH}_3\text{COH} + \text{OH}$ (R46) with a barrier of $26.7 \text{ kcal mol}^{-1}$. The third is H-abstraction by O_2 leading to $\text{CH}_3\text{COOH} + \text{HO}_2$ (R47) with a barrier of $26.2 \text{ kcal mol}^{-1}$. On the basis of the calculated reaction barriers, β -site $\text{C}_1\text{--C}_2$ bond scission is the dominant pathway in the fragmentation of the $\text{HOCH}(\text{CH}_3)\text{O}$ radical. This conclusion is further supported by the previous experimental result that β -hydroxy intermediates primarily undergo decomposition rather than react with O_2 in the presence of NO (Aschmann et al., 2000). Equivalent to the $\text{HOCH}(\text{CH}_3)\text{OO} + \text{NO}$ reaction, the bimolecular reaction of $\text{HO}(\text{CH}_3)_2\text{COO}$ radicals with NO has similar transformation pathways (Fig. 12). The reaction of $\text{HO}(\text{CH}_3)_2\text{COO}$ with NO initially proceeds via a barrierless addition leading to S35-*cis* with a binding energy of $12.6 \text{ kcal mol}^{-1}$. Then, S35-*cis* fragments into an $\text{HO}(\text{CH}_3)_2\text{CO}$ radical and NO_2 (R50) via the cleavage of the $\text{O}_2\text{--O}_3$ bond with a barrier of $11.4 \text{ kcal mol}^{-1}$. The formed $\text{HO}(\text{CH}_3)_2\text{CO}$ radical can either dissociate into $\text{CH}_3\text{COOH} + \text{CH}_3$ (R51) via the scission of the $\text{C}_1\text{--C}_3$ bond with a barrier of $8.2 \text{ kcal mol}^{-1}$, or decompose into $\text{CH}_3\text{COCH}_3 + \text{OH}$ (R52) through the cleavage of the $\text{C}_1\text{--O}_1$ bond with a barrier of $24.3 \text{ kcal mol}^{-1}$. This result also shows that β -site C–C bond scission is the dominant pathway.

The typical atmospheric concentrations of NO are around 10, 1, and 20 pptv in urban, rural, and forest environments, respectively (Bianchi et al., 2019). The rate coefficient of HOCH_2OO radical reaction with NO is calculated to be $4.3 \times 10^{-12} \text{ cm}^3 \text{ molecule}^{-1} \text{ s}^{-1}$ at room temperature, resulting in the pseudo-first-order rate constants $k'_{\text{NO}} = k_{\text{NO}}[\text{NO}]$ of 6.5×10^{-1} , 6.5×10^{-2} , and 1.3×10^{-3} , respectively, in urban, rural, and forest environments. It is of interest to assess the relative importance for the H-shift reaction of HOCH_2OO radicals and bimolecular reactions with HO_2 radicals and NO based on the calculated $k_{\text{MC-TST}}$, k'_{HO_2} , and k'_{NO} . It is found that the H-shift reaction is of less importance, the HO_2 radical reaction is favorable in forest environments, and the

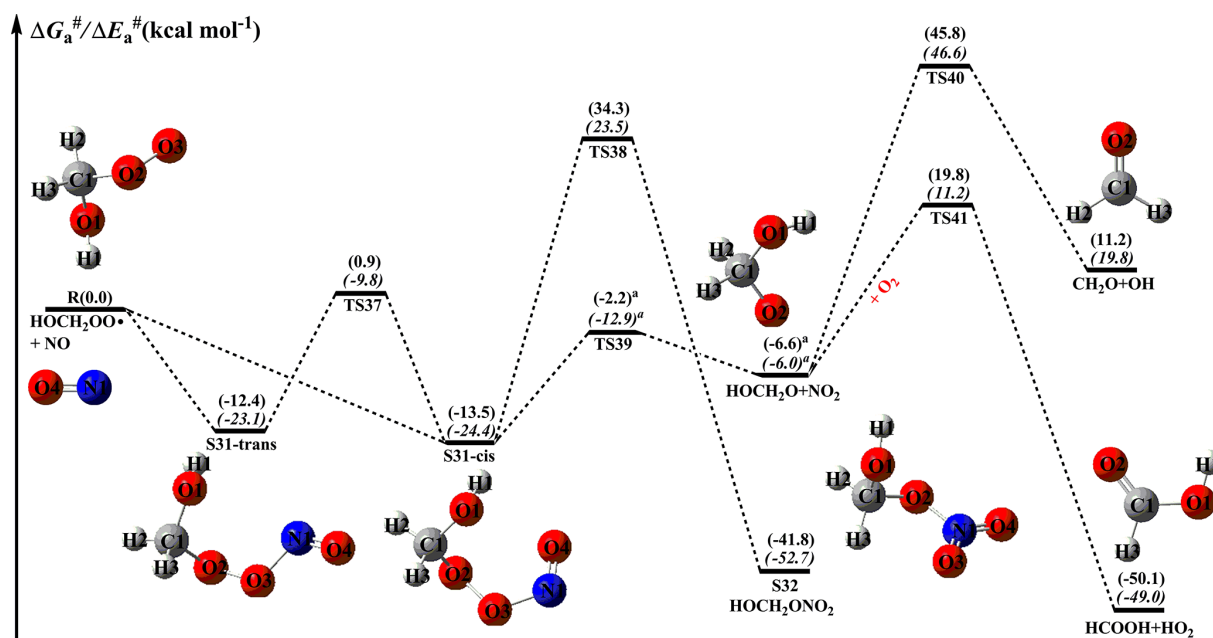


Figure 10. PES ($\Delta G_a^\#$ and $\Delta E_a^\#$, in italics) for the reaction of an $\text{HOCH}_2\text{OO}^\bullet$ radical with NO predicted at the M06-2X/ma-TZVP//M06-2X/6-311+G(2df,2p) level of theory (the superscript a is calculated at the MP2/ma-TZVP//MP2/6-311+G(2df,2p) level).

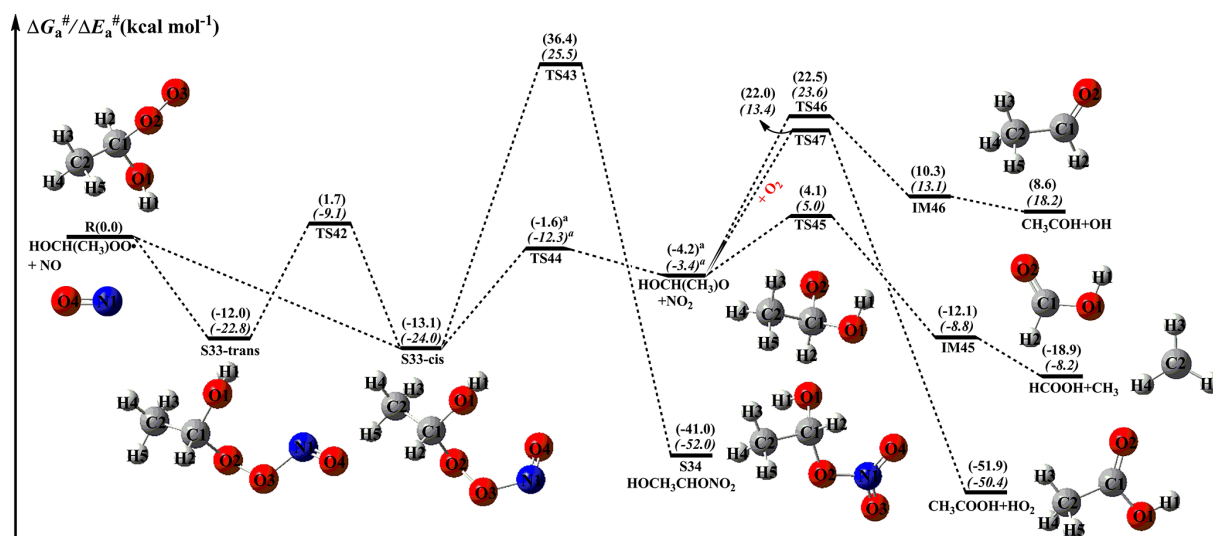


Figure 11. PES ($\Delta G_a^\#$ and $\Delta E_a^\#$, in italics) for the reaction of an $\text{HOCH}(\text{CH}_3)\text{OO}^\bullet$ radical with NO predicted at the M06-2X/ma-TZVP//M06-2X/6-311+G(2df,2p) level of theory (the superscript a is calculated at the MP2/ma-TZVP//MP2/6-311+G(2df,2p) level).

NO reaction is predominant in urban and rural environments. A similar conclusion was also obtained from the cases of $\text{HOCH}(\text{CH}_3)\text{OO}$ and $\text{HO}(\text{CH}_3)_2\text{CHOO}$ radicals.

The rate coefficients of the dominant pathways of HOCH_2O , $\text{HOCH}(\text{CH}_3)\text{O}$, and $\text{HO}(\text{CH}_3)_2\text{CHO}$ radical fragmentations are summarized in Table S12 in the Supplement. As can be seen in Table S12, k_{R41} increases slightly with increasing temperature, and the discrepancy is about a factor of 12 at the two extremes of the studied temperature range.

At the ground level with $[\text{O}_2] = \sim 5.0 \times 10^{18} \text{ molecule cm}^{-3}$, the pseudo-first-order rate constant $k'_{\text{O2}} = k_{\text{R41}}[\text{O}_2]$ is estimated to be 38.0 s^{-1} at room temperature. k_{R45} varies significantly from 2.0×10^6 (273 K) to 3.1×10^8 (400 K) s^{-1} , and it exhibits a marked positive temperature dependence. A similar phenomenon is observed for k_{R51} : it increases significantly with increasing temperature. k_{R51} is greater than k_{R45} by a factor of ~ 1.3 , suggesting that the rate coefficient of β -

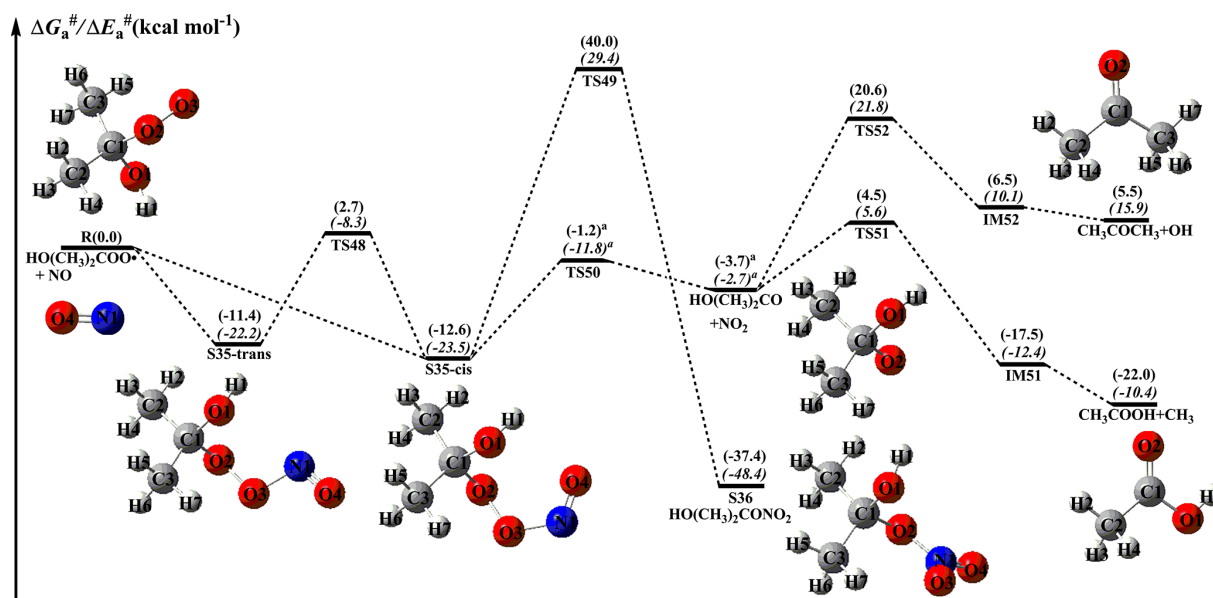


Figure 12. PES (ΔG_a^\ddagger and ΔE_a^\ddagger , in italics) for the reaction of an $\text{HO}(\text{CH}_3)_2\text{COO}^\bullet$ radical with NO predicted at the M06-2X/ma-TZVP//M06-2X/6-311+G(2df,2p) level of theory (the superscript a is calculated at the MP2/ma-TZVP//MP2/6-311+G(2df,2p) level).

site C–C bond scission increases slightly when the number of methyl groups increases.

4 Conclusions

The detailed mechanisms and kinetic properties of OH-initiated oxidation of distinct HHPs and the subsequent transformation of resulting H-abstraction products are investigated using quantum chemical and kinetics modeling methods. The main conclusions are summarized as follows.

(a) The dominant pathway is H-abstraction from the -OOH group in the initiation reactions of OH radicals with HOCH_2OOH and $\text{HOC}(\text{CH}_3)_2\text{OOH}$. H-abstraction from the -CH group is competitive with that from the -OOH group in the reaction of OH radicals with $\text{HOCH}(\text{CH}_3)\text{OOH}$. The barrier of H-abstraction from the -OOH group slightly increases when the number of methyl groups increases. Compared with the rate coefficient of the dominant pathway in the parent system, it is almost identical when a methyl group substitution occurs at the C_1 -position, whereas it reduces by a factor of 2–5 when two methyl groups are introduced at the C_1 -position. The atmospheric lifetimes of HOCH_2OOH , $\text{HOCH}(\text{CH}_3)\text{OOH}$, and $\text{HOC}(\text{CH}_3)_2\text{OOH}$ reactivity toward OH radicals are estimated to be 0.58–1.74, 0.60–1.79, and 1.23–3.69 h, respectively, at room temperature under the typical OH radical concentrations of $5\text{--}15 \times 10^6 \text{ molecules cm}^{-3}$ during daylight.

(b) The self-reaction of RO_2 radicals initially produces a tetroxide intermediate via oxygen-to-oxygen coupling, and then it decomposes into propagation and termination products through asymmetric two-step O–O bond scission. The

rate-limiting step is the first O–O bond cleavage, and the barrier increases when the number of methyl groups increases. This finding contributes toward the understanding of the self-reaction of complex RO_2 radicals.

(c) The bimolecular reactions of distinct RO_2 radicals with HO_2 radicals lead to the formation of hydroperoxide ROOH as the main product, and the barrier height is not affected by the number of methyl substitutions. Compared with the rate coefficient for the $\text{HOCH}_2\text{OO} + \text{HO}_2$ reaction, the rate coefficients increase by a factor of 2–5 when one or two methyl groups are introduced at the C_1 -position. Using an HO_2 radical concentration of $\sim 50 \text{ pptv}$ in forest environments, the pseudo-first-order rate constants k'_{HO_2} of the reactions of distinct RO_2 radicals with an HO_2 radical vary from 1 to $5 \times 10^{-2} \text{ s}^{-1}$.

(d) The isomerization reactions of HOCH_2OO , $\text{HOCH}(\text{CH}_3)\text{OO}$, and $\text{HO}(\text{CH}_3)_2\text{COO}$ radicals are unlikely to proceed in the atmosphere because the intramolecular H-shift steps have considerably high barriers and are strongly endergonic. The result suggests that the isomerization of RO_2 radicals with small carbon structures is of less importance in the atmosphere.

(e) The reaction with O_2 to form formic acid and an HO_2 radical is the dominant removal pathway for HOCH_2O radicals formed from the reaction of an HOCH_2OO radical with NO . β -site C–C bond scission is the dominant pathway in the dissociation of $\text{HOCH}(\text{CH}_3)\text{O}$ and $\text{HOC}(\text{CH}_3)_2\text{O}$ radicals formed from the reactions of NO with $\text{HOCH}(\text{CH}_3)\text{OO}$ and $\text{HOC}(\text{CH}_3)_2\text{OO}$ radicals. The result suggests that methyl-substituted alkoxy radicals primarily proceed via β -site C–C bond scission to produce aldehyde or carbonyl.

Data availability. The data are accessible by contacting the corresponding author (huangyu@ieecas.cn).

Supplement. The following information is provided in the Supplement: Y//X (Y = M06-2X, CCSD (T), X = 6-311+G(2df,2p), ma-TZVP) calculated energy barrier (ΔE_a^\ddagger , ΔG_a^\ddagger) for the OH + HHPs reactions; rate coefficients of each elementary pathway involved in the initiation reactions of OH radicals with HOCH₂OOH, HOCH(CH₃)OOH, and HO(CH₃)₂COOH; rate coefficients of HO₂ radical reactions with HOCH₂OO, HOCH(CH₃)OO, and HO(CH₃)₂COO radicals; the relative free energy and Boltzmann populations (w_i) of the conformer of HOCH₂OO, HOCH(CH₃)OO, and HO(CH₃)₂COO radicals; the single-conformer rate coefficients ($k_{\text{IRC-TST}}$) and multi-conformer rate coefficients ($k_{\text{MC-TST}}$) of HOCH₂OO, HOCH(CH₃)OO, and HO(CH₃)₂COO radicals; rate coefficients of dominant pathways in the HOCH₂OO• + NO, HOCH(CH₃)OO• + NO, and HO(CH₃)₂CHOO• + NO reactions; PESs (ΔE_a^\ddagger) for the OH-initiated reactions of HOCH₂OOH, HOCH(CH₃)OOH, and HO(CH₃)₂OOH; geometries of all stationary points; plots of the rate coefficients of each elementary pathway versus temperature; PESs (ΔG_a^\ddagger and ΔE_a^\ddagger , in italics) for the isomerization of HOCH(CH₃)OO and HO(CH₃)₂COO radicals. The supplement related to this article is available online at: <https://doi.org/10.5194/acp-22-3693-2022-supplement>.

Author contributions. LC designed the study. LC and YH wrote the paper. LC performed theoretical calculation. YX, ZJ, and WW analyzed the data. All authors reviewed and commented on the paper.

Competing interests. The contact author has declared that neither they nor their co-authors have any competing interests

Disclaimer. Publisher's note: Copernicus Publications remains neutral with regard to jurisdictional claims in published maps and institutional affiliations.

Acknowledgements. This work was supported by the National Natural Science Foundation of China (grant nos. 42175134, 41805107, and 22002080). It was also partially supported as Key Projects of Chinese Academy of Sciences, China (grant no. ZDRW-ZS-2017-6), Strategic Priority Research Program of the Chinese Academy of Sciences, China (grant nos. XDA23010300 and XDA23010000), Key Project of International Cooperation of the Chinese Academy of Sciences, China (grant no. GJHZ1543), Research Grants Council of Hong Kong, China (grant no. PolyU 152083/14E), CAS "Light of West China" Program (XAB2019B01), and the General Project of Shaanxi Province (2020JQ-432).

Financial support. This research has been supported by the National Natural Science Foundation of China (grant nos. 42175134, 41805107, and 22002080). It was also partially supported as Key Projects of the Chinese Academy of Sciences, China (grant no. ZDRW-ZS-2017-6), Strategic Priority Research Program of the Chinese Academy of Sciences, China (grant nos. XDA23010300 and XDA23010000), Key Project of International Cooperation of the Chinese Academy of Sciences, China (grant no. GJHZ1543), Research Grants Council of Hong Kong, China (grant no. PolyU 152083/14E), CAS "Light of West China" Program (grant no. XAB2019B01), and the General Project of Shaanxi Province (grant no. 2020JQ-432).

Review statement. This paper was edited by Arthur Chan and reviewed by three anonymous referees.

References

- Allen, H. M., Crounse, J. D., Bates, K. H., Teng, A. P., Krawiec-Thayer, M. P., Rivera-Rios, J. C., Keutsch, F. N., Clair, J. M. S., Hanisco, T. F., Møller, K. H., Kjaergaard, H. G., and Wennberg, P. O.: Kinetics and product yields of the OH initiated oxidation of hydroxymethyl hydroperoxide, *J. Phys. Chem. A*, 122, 6292–6302, <https://doi.org/10.1021/acs.jpca.8b04577>, 2018.
- Anglada, J. M. and Solé, A.: Impact of the water dimer on the atmospheric reactivity of carbonyl oxides, *Phys. Chem. Chem. Phys.*, 18, 17698–17712, <https://doi.org/10.1039/C6CP02531E>, 2016.
- Anglada, J. M., González, J., and Torrent-Sucarrat, M.: Effects of the substituents on the reactivity of carbonyl oxides. A theoretical study on the reaction of substituted carbonyl oxides with water, *Phys. Chem. Chem. Phys.*, 13, 13034–13045, <https://doi.org/10.1039/c1cp20872a>, 2011.
- Aschmann, S. M., Arey, J., and Atkinson, R.: Formation of β -hydroxycarbonyls from the OH radical-initiated reactions of selected alkenes, *Environ. Sci. Technol.*, 34, 1702–1706, <https://doi.org/10.1021/es991125a>, 2000.
- Atkinson, R. and Arey, J.: Atmospheric degradation of volatile organic compounds, *Chem. Rev.*, 103, 4605–4638, <https://doi.org/10.1021/cr0206420>, 2003.
- Bach, R. D., Dmitrenko, O., and Estévez, C. M.: Chemical behavior of the biradicaloid (HO••ONO) singlet states of peroxyxynitrous acid. The oxidation of hydrocarbons, sulfides, and selenides, *J. Am. Chem. Soc.*, 127, 3140–3155, <https://doi.org/10.1021/ja044245d>, 2005.
- Berndt, T., Richters, S., Kaethner, R., Voigtländer, J., Stratmann, F., Sipilä, M., Kulmala, M., and Herrmann, H.: Gas-phase ozonolysis of cycloalkenes: formation of highly oxidized RO₂ radicals and their reactions with NO, NO₂, SO₂, and other RO₂ radicals, *J. Phys. Chem. A*, 119, 10336–10348, <https://doi.org/10.1021/acs.jpca.5b07295>, 2015.
- Berndt, T., Scholz, W., Mentler, B., Fischer, L., Herrmann, H., Kulmala, M., and Hansel, A.: Accretion product formation from self- and cross-reactions of RO₂ radicals in the atmosphere, *Angew. Chem. Int. Edit.*, 57, 3820–3824, <https://doi.org/10.1002/anie.201710989>, 2018.
- Bianchi, F., Kurten, T., Riva, M., Mohr, C., Rissanen, M. P., Roldin, P., Berndt, T., Crounse, J. D., Wennberg, P. O., Mentel, T. F.,

- Wildt, J., Junninen, H., Jokinen, T., Kulmala, M., Worsnop, D. R., Thornton, J. A., Donahue, N., Kjaergaard, H. G., and Ehn, M.: Highly oxygenated organic molecules (HOM) from gas-phase autoxidation involving peroxy radicals: a key contributor to atmospheric aerosol, *Chem. Rev.*, 119, 3472–3509, <https://doi.org/10.1021/acs.chemrev.8b00395>, 2019.
- Boys, S. F. and Bernardi, F.: The calculation of small molecular interactions by the differences of separate total energies. Some procedures with reduced errors, *Mol. Phys.*, 19, 553–566, <https://doi.org/10.1080/00268977000101561>, 1970.
- Chao, W., Hsieh, J. T., Chang, C. H., and Lin, J. J. M.: Direct kinetic measurement of the reaction of the simplest Criegee intermediate with water vapor, *Science*, 347, 751–754, <https://doi.org/10.1126/science.1261549>, 2015.
- Chen, L., Wang, W., Zhou, L., Wang, W., Liu, F., Li, C., and Lü, J.: Role of water clusters in the reaction of the simplest Criegee intermediate CH_2OO with water vapour, *Theor. Chem. Acc.*, 135, 252–263, <https://doi.org/10.1007/s00214-016-1998-2>, 2016a.
- Chen, L., Wang, W., Wang, W., Liu, Y., Liu, F., Liu, N., and Wang, B.: Water-catalyzed decomposition of the simplest Criegee intermediate CH_2OO , *Theor. Chem. Acc.*, 135, 131–143, <https://doi.org/10.1007/s00214-016-1894-9>, 2016b.
- Chen, L., Huang, Y., Xue, Y., Cao, J., and Wang, W.: Competition between HO_2 and H_2O_2 reactions with CH_2OO /*anti*- CH_3CHOO in the oligomer formation: a theoretical perspective, *J. Phys. Chem. A*, 121, 6981–6991, <https://doi.org/10.1021/acs.jpca.7b05951>, 2017.
- Chen, L., Huang, Y., Xue, Y., Shen, Z., Cao, J., and Wang, W.: Mechanistic and kinetics investigations of oligomer formation from Criegee intermediate reactions with hydroxyalkyl hydroperoxides, *Atmos. Chem. Phys.*, 19, 4075–4091, <https://doi.org/10.5194/acp-19-4075-2019>, 2019.
- Chen, L., Huang, Y., Xue, Y., Jia, Z., and Wang, W.: Atmospheric oxidation of 1-butene initiated by OH radical: Implications for ozone and nitrous acid formations, *Atmos. Environ.*, 244, 118010–118021, <https://doi.org/10.1016/j.atmosenv.2020.118010>, 2021.
- Chhantyal-Pun, R., Welz, O., Savee, J. D., Eskola, A. J., Lee, E. P. F., Blacker, L., Hill, H. R., Ashcroft, M., Khan, M. A. H., Lloyd-Jones, G. C., Evans, L., Rotavera, B., Huang, H., Osborn, D. L., Mok, D. K. W., Dyke, J. M., Shallcross, D. E., Percival, C. J., Orr-Ewing, A. J., and Taatjes, C. A.: Direct measurements of unimolecular and bimolecular reaction kinetics of the Criegee intermediate $(\text{CH}_3)_2\text{COO}$, *J. Phys. Chem. A*, 121, 4–15, <https://doi.org/10.1021/acs.jpca.6b07810>, 2017.
- Crounse, J. D., Nielsen, L. B., Jørgensen, S., Kjaergaard, H. G., and Wennberg, P. O.: Autoxidation of organic compounds in the atmosphere, *J. Phys. Chem. Lett.*, 4, 3513–3520, <https://doi.org/10.1021/jz4019207>, 2013.
- Dillon, T. J. and Crowley, J. N.: Direct detection of OH formation in the reactions of HO_2 with $\text{CH}_3\text{C}(\text{O})\text{O}_2$ and other substituted peroxy radicals, *Atmos. Chem. Phys.*, 8, 4877–4889, <https://doi.org/10.5194/acp-8-4877-2008>, 2008.
- Eckart, C.: The penetration of a potential barrier by electrons, *Phys. Rev.*, 35, 1303–1309, <https://doi.org/10.1103/PhysRev.35.1303>, 1930.
- Ehn, M., Thornton, J. A., Kleist, E., Sipilä, M., Junninen, H., Pullinen, I., Springer, M., Rubach, F., Tillmann, R., Lee, B., Lopez-Hilfiker, F., Andres, S., Acir, I. H., Rissanen, M., Jokinen, T., Schobesberger, S., Kangasluoma, J., Kontkanen, J., Nieminen, T., Kurtén, T., Nielsen, L. B., Jørgensen, S., Kjaergaard, H. G., Canagaratna, M., Maso, M. D., Berndt, T., Petäjä, T., Wahner, A., Kerminen, V. M., Kulmala, M., Worsnop, D. R., Wildt, J., and Mentel, T. F.: A large source of low-volatility secondary organic aerosol, *Nature*, 506, 476–479, <https://doi.org/10.1038/nature13032>, 2014.
- Ehn, M., Berndt, T., Wildt, J., and Mentel, T.: Highly oxygenated molecules from atmospheric autoxidation of hydrocarbons: a prominent challenge for chemical kinetics studies, *Int. J. Chem. Kinet.*, 49, 821–831, <https://doi.org/10.1002/kin.21130>, 2017.
- Fernández-Ramos, A., Ellingson, B. A., Meana-Pañeda, R., Marques, J. M. C., and Truhlar, D. G.: Symmetry numbers and chemical reaction rates, *Theor. Chem. Acc.*, 118, 813–826, <https://doi.org/10.1007/s00214-007-0328-0>, 2007.
- Francisco, J. S. and Eisfeld, W.: Atmospheric oxidation mechanism of hydroxymethyl hydroperoxide, *J. Phys. Chem. A*, 113, 7593–7600, <https://doi.org/10.1021/jp901735z>, 2009.
- Frisch, M. J., Trucks, G. W., Schlegel, H. B., Scuseria, G. E., Robb, M. A., Cheeseman, J. R., Montgomery, J. A. Jr., Vreven, T., Kudin, K. N., Burant, J. C., Millam, J. M., Iyengar, S. S., Tomasi, J., Barone, V., Mennucci, B., Cossi, M., Scalmani, G., Rega, N., Petersson, G. A., Nakatsuji, H., Hada, M., Ehara, M., Toyota, K., Fukuda, R., Hasegawa, J., Ishida, M., Nakajima, T., Honda, Y., Kitao, O., Nakai, H., Klene, M., Li, X., Knox, J. E., Hratchian, H. P., Cross, J. B., Adamo, C., Jaramillo, J., Gomperts, R., Stratmann, R. E., Yazyev, O., Austin, A. J., Cammi, R., Pomelli, C., Ochterski, J. W., Ayala, P. Y., Morokuma, K., Voth, G. A., Salvador, P., Dannenberg, J. J., Zakrzewski, V. G., Dapprich, S., Daniels, A. D., Strain, M. C., Farkas, O., Malick, D. K., Rabuck, A. D., Raghavachari, K., Foresman, J. B., Ortiz, J. V., Cui, Q., Baboul, A. G., Clifford, S., Cioslowski, J., Stefanov, B. B., Liu, G., Liashenko, A., Piskorz, P., Komaromi, I., Martin, R. L., Fox, D. J., Keith, T., Al-Laham, M. A., Peng, C. Y., Nanayakkara, A., Challacombe, M., Gill, P. M. W., Johnson, B., Chen, W., Wong, M. W., Gonzalez, C., and Pople, J. A.: Gaussian 09, Revision D.01, Gaussian, Inc., Wallingford, CT, <http://www.gaussian.com> (last access: 9 February 2022), 2009.
- Fukui, K.: The path of chemical reactions – the IRC approach, *Accounts Chem. Res.*, 14, 363–368, <https://doi.org/10.1021/ar00072a001>, 1981.
- Gilbert, R. G. and Smith, S. C.: Theory of unimolecular and recombination reactions, Blackwell Scientific, Carlton, Australia, ISBN 0632027495, 1990.
- Gligorovski, S., Strekowski, R., Barbati, S., and Vione, D.: Environmental implications of hydroxyl radicals ($\cdot\text{OH}$), *Chem. Rev.*, 115, 13051–13092, <https://doi.org/10.1021/cr500310b>, 2015.
- Glowacki, D. R., Liang, C. H., Morley, C., Pilling, M. J., and Robertson, S. H.: MESMER: an open-source master equation solver for multi-energy well reactions, *J. Phys. Chem. A*, 116, 9545–9560, <https://doi.org/10.1021/jp3051033>, 2012.
- Gong, Y. and Chen, Z.: Quantification of the role of stabilized Criegee intermediates in the formation of aerosols in limonene ozonolysis, *Atmos. Chem. Phys.*, 21, 813–829, <https://doi.org/10.5194/acp-21-813-2021>, 2021.
- Hofzumahaus, A., Rohrer, F., Lu, K., Bohn, B., Brauers, T., Chang, C. C., Fuchs, H., Holland, F., Kita, K., Kondo, Y., Li, X., Lou, S., Shao, M., Zeng, L., Wahner, A., and Zhang, Y.: Amplified

- trace gas removal in the troposphere, *Science*, 324, 1702–1704, <https://doi.org/10.1126/science.1164566>, 2009.
- Holbrook, K. A., Pilling, M. J., Robertson, S. H., and Robinson, P. J.: Unimolecular reactions, 2nd edn., Wiley, New York, ISBN 0-471-92268-4, 1996.
- Huang, H. L., Chao, W., and Lin, J. J. M.: Kinetics of a Criegee intermediate that would survive high humidity and may oxidize atmospheric SO₂, *P. Natl. Acad. Sci. USA*, 112, 10857–10862, <https://doi.org/10.1073/pnas.1513149112>, 2015.
- Iyer, S., Reiman, H., Møller, K. H., Rissanen, M. P., Kjaergaard, H. G., and Kurtén, T.: Computational investigation of RO₂ + HO₂ and RO₂ + RO₂ reactions of monoterpene derived first-generation peroxy radicals leading to radical recycling, *J. Phys. Chem. A*, 122, 9542–9552, <https://doi.org/10.1021/acs.jpca.8b09241>, 2018.
- Iyer, S., Rissanen, M. P., Valiev, R., Barua, S., Krechmer, J. E., Thornton, J., Ehn, M., and Kurtén, T.: Molecular mechanism for rapid autoxidation in α -pinene ozonolysis, *Nat. Commun.*, 12, 878–883, <https://doi.org/10.1038/s41467-021-21172-w>, 2021.
- Jara-Toro, R. A., Hernández, F. J., Taccone, R. A., Lane, S. I., and Pino, G. A.: Water catalysis of the reaction between methanol and OH at 294 K and the atmospheric implications, *Angew. Chem. Int. Edit.*, 56, 2166–2170, <https://doi.org/10.1002/anie.201612151>, 2017.
- Jara-Toro, R. A., Hernández, F. J., Garavagno, M. A., Taccone, R. A., and Pino, G. A.: Water catalysis of the reaction between hydroxyl radicals and linear saturated alcohols (ethanol and *n*-propanol) at 294 K, *Phys. Chem. Chem. Phys.*, 20, 27885–27896, <https://doi.org/10.1039/C8CP05411H>, 2018.
- Jokinen, T., Sipilä, M., Richters, S., Kerminen, V. M., Paasonen, P., Stratmann, F., Worsnop, D., Kulmala, M., Ehn, M., Herrmann, H., and Berndt, T.: Rapid autoxidation forms highly oxidized RO₂ radicals in the atmosphere, *Angew. Chem. Int. Edit.*, 53, 14596–14600, <https://doi.org/10.1002/anie.201408566>, 2014.
- Khan, M. A. H., Percival, C. J., Caravan, R. L., Taatjes, C. A., and Shallcross, D. E.: Criegee intermediates and their impacts on the troposphere, *Environ. Sci.-Proc. Imp.*, 20, 437–453, <https://doi.org/10.1039/C7EM00585G>, 2018.
- Kumar, M. and Francisco, J. S.: Red-light-induced decomposition of an organic peroxy radical: a new source of the HO₂ radical, *Angew. Chem. Int. Edit.*, 54, 15711–15714, <https://doi.org/10.1002/anie.201509311>, 2015.
- Kumar, M. and Francisco, J. S.: Red-light initiated decomposition of α -hydroxy methylperoxy radical in the presence of organic and inorganic acids: implications for the HO_x formation in the lower stratosphere, *J. Phys. Chem. A*, 120, 2677–2683, <https://doi.org/10.1021/acs.jpca.6b01515>, 2016.
- Kumar, M., Busch, D. H., Subramaniam, B., and Thompson, W. H.: Role of tunable acid catalysis in decomposition of α -hydroxyalkyl hydroperoxides and mechanistic implications for tropospheric chemistry, *J. Phys. Chem. A*, 118, 9701–9711, <https://doi.org/10.1021/jp505100x>, 2014.
- Lee, R., Gryn'ova, G., Ingold, K. U., and Coote, M. L.: Why are sec-alkylperoxyl bimolecular self-reactions orders of magnitude faster than the analogous reactions of tert-alkylperoxyls? The unanticipated role of CH hydrogen bond donation, *Phys. Chem. Chem. Phys.*, 18, 23673–23679, <https://doi.org/10.1039/C6CP04670C>, 2016.
- Lester, M. I. and Klippenstein, S. J.: Unimolecular decay of Criegee intermediates to OH radical products: prompt and thermal decay processes, *Accounts Chem. Res.*, 51, 978–985, <https://doi.org/10.1021/acs.accounts.8b00077>, 2018.
- Liu, L., Bei, N., Wu, J., Liu, S., Zhou, J., Li, X., Yang, Q., Feng, T., Cao, J., Tie, X., and Li, G.: Effects of stabilized Criegee intermediates (sCIs) on sulfate formation: a sensitivity analysis during summertime in Beijing–Tianjin–Hebei (BTH), China, *Atmos. Chem. Phys.*, 19, 13341–13354, <https://doi.org/10.5194/acp-19-13341-2019>, 2019.
- Long, B., Bao, J. L., and Truhlar, D. G.: Reaction of SO₂ with OH in the atmosphere, *Phys. Chem. Chem. Phys.*, 19, 8091–8100, <https://doi.org/10.1039/C7CP00497D>, 2017.
- Lu, T.: Molclus program, Version 1.9.3, <http://www.keinsci.com/research/molclus.html>, last access: 10 February 2020.
- Ma, F., Guo, X., Xia, D., Xie, H. B., Wang, Y., Elm, J., Chen, J., and Niu, J.: Atmospheric chemistry of allylic radicals from isoprene: a successive cyclization-driven autoxidation mechanism, *Environ. Sci. Technol.*, 55, 4399–4409, <https://doi.org/10.1021/acs.est.0c07925>, 2021.
- Møller, K. H., Otkjær, R. V., Hyttinen, N., Kurtén, T., and Kjaergaard, H. G.: Cost-effective implementation of multi-conformer transition state theory for peroxy radical hydrogen shift reactions, *J. Phys. Chem. A*, 120, 10072–10087, <https://doi.org/10.1021/acs.jpca.6b09370>, 2016.
- Møller, K. H., Berndt, T., and Kjaergaard, H. G.: Atmospheric autoxidation of amines, *Environ. Sci. Technol.*, 54, 11087–11099, <https://doi.org/10.1021/acs.est.0c03937>, 2020.
- Nozière, B. and Vereecken, L.: Direct observation of aliphatic peroxy radical autoxidation and water effects: an experimental and theoretical study, *Angew. Chem. Int. Edit.*, 58, 13976–13982, <https://doi.org/10.1002/anie.201907981>, 2019.
- Orlando, J. J. and Tyndall, G. S.: Laboratory studies of organic peroxy radical chemistry: an overview with emphasis on recent issues of atmospheric significance, *Chem. Soc. Rev.*, 41, 6294–6317, <https://doi.org/10.1039/c2cs35166h>, 2012.
- Perring, A. E., Pusede, S. E., and Cohen, R. C.: An observational perspective on the atmospheric impacts of alkyl and multifunctional nitrates on ozone and secondary organic aerosol, *Chem. Rev.*, 113, 5848–5870, <https://doi.org/10.1021/cr300520x>, 2013.
- Piletic, I. R., Edney, E. O., and Bartolotti, L. J.: Barrierless reactions with loose transition states govern the yields and lifetimes of organic nitrates derived from isoprene, *J. Phys. Chem. A*, 121, 8306–8321, <https://doi.org/10.1021/acs.jpca.7b08229>, 2017.
- Qiu, J. T., Ishizuka, S., Tonokura, K., Colussi, A. J., and Enami, S.: Water dramatically accelerates the decomposition of α -hydroxyalkyl-hydroperoxides in aerosol particles, *J. Phys. Chem. Lett.*, 10, 5748–5755, <https://doi.org/10.1021/acs.jpclett.9b01953>, 2019.
- Rissanen, M. P., Kurtén, T., Sipilä, M., Thornton, J. A., Kangasluoma, J., Sarnela, N., Junninen, H., Jørgensen, S., Schallhart, S., Kajos, M. K., Taipale, R., Springer, M., Mentel, T. F., Ruuskanen, T., Petäjä, T., Worsnop, D. R., Kjaergaard, H. G., and Ehn, M.: The formation of highly oxidized multifunctional products in the ozonolysis of cyclohexene, *J. Am. Chem. Soc.*, 136, 15596–15606, <https://doi.org/10.1021/ja507146s>, 2014.
- Russell, G. A.: Deuterium-isotope effects in the autoxidation of aralkyl hydrocarbons. Mechanism of the interaction

- of peroxy radicals, *J. Am. Chem. Soc.*, 79, 3871–3877, <https://doi.org/10.1021/ja01571a068>, 1957.
- Ryzhkov, A. B. and Ariya, P. A.: A theoretical study of the reactions of carbonyl oxide with water in atmosphere: the role of water dimer, *Chem. Phys. Lett.*, 367, 423–429, [https://doi.org/10.1016/S0009-2614\(02\)01685-8](https://doi.org/10.1016/S0009-2614(02)01685-8), 2003.
- Smith, M. C., Chang, C. H., Chao, W., Lin, L. C., Takahashi, K., Boering, K. A., and Lin, J. J. M.: Strong negative temperature dependence of the simplest Criegee intermediate CH_2OO reaction with water dimer, *J. Phys. Chem. Lett.*, 6, 2708–2713, <https://doi.org/10.1021/acs.jpcllett.5b01109>, 2015.
- Stone, D., Whalley, L. K., and Heard, D. E.: Tropospheric OH and HO_2 radicals: field measurements and model comparisons, *Chem. Soc. Rev.*, 41, 6348–6404, <https://doi.org/10.1039/c2cs35140d>, 2012.
- Taatjes, C. A.: Criegee intermediates: what direct production and detection can teach us about reactions of carbonyl oxides, *Annu. Rev. Phys. Chem.*, 68, 183–207, <https://doi.org/10.1146/annurev-physchem-052516-050739>, 2017.
- Taatjes, C. A., Welz, O., Eskola, A. J., Savee, J. D., Scheer, A. M., Shallcross, D. E., Rotavera, B., Lee, E. P. F., Dyke, J. M., Mok, D. K. W., Osborn, D. L., and Percival, C. J.: Direct measurements of conformer-dependent reactivity of the Criegee intermediate CH_3CHOO , *Science*, 340, 177–180, <https://doi.org/10.1126/science.1234689>, 2013.
- Valiev, R. R., Hasan, G., Salo, V. T., Kubečka, J., and Kurten, T.: Intersystem crossings drive atmospheric gas-phase dimer formation, *J. Phys. Chem. A*, 123, 6596–6604, <https://doi.org/10.1021/acs.jpca.9b02559>, 2019.
- Wang, S., Wu, R., Berndt, T., Ehn, M., and Wang, L.: Formation of highly oxidized radicals and multifunctional products from the atmospheric oxidation of alkylbenzenes, *Environ. Sci. Technol.*, 51, 8442–8449, <https://doi.org/10.1021/acs.est.7b02374>, 2017.
- Wang, S., Riva, M., Yan, C., Ehn, M., and Wang, L.: Primary formation of highly oxidized multifunctional products in the OH-initiated oxidation of isoprene: a combined theoretical and experimental study, *Environ. Sci. Technol.*, 52, 12255–12264, <https://doi.org/10.1021/acs.est.8b02783>, 2018.
- Wennberg, P. O., Bates, K. H., Crounse, J. D., Dodson, L. G., McVay, R. C., Mertens, L. A., Nguyen, T. B., Praske, E., Schwantes, R. H., Smarte, M. D., Clair, J. M. S., Teng, A. P., Zhang, X., and Seinfeld, J. H.: Gas-phase reactions of isoprene and its major oxidation products, *Chem. Rev.*, 118, 3337–3390, <https://doi.org/10.1021/acs.chemrev.7b00439>, 2018.
- Winiberg, F. A. F., Dillon, T. J., Orr, S. C., Groß, C. B. M., Bejan, I., Brumby, C. A., Evans, M. J., Smith, S. C., Heard, D. E., and Seakins, P. W.: Direct measurements of OH and other product yields from the $\text{HO}_2 + \text{CH}_3\text{C(O)O}_2$ reaction, *Atmos. Chem. Phys.*, 16, 4023–4042, <https://doi.org/10.5194/acp-16-4023-2016>, 2016.
- Xu, L., Kollman, M. S., Song, C., Shilling, J. E., and Ng, N. L.: Effects of NO_x on the volatility of secondary organic aerosol from isoprene photooxidation, *Environ. Sci. Technol.*, 48, 2253–2262, <https://doi.org/10.1021/es404842g>, 2014.
- Xu, L., Møller, K. H., Crounse, J. D., Kjaergaard, H. G., and Wennberg, P. O.: New insights into the radical chemistry and product distribution in the OH-initiated oxidation of benzene, *Environ. Sci. Technol.*, 54, 13467–13477, <https://doi.org/10.1021/acs.est.0c04780>, 2020.
- Zhang, D., Zhang, R., Park, J., and North, S. W.: Hydroxy peroxy nitrites and nitrates from OH initiated reactions of isoprene, *J. Am. Chem. Soc.*, 124, 9600–9605, <https://doi.org/10.1021/ja0255195>, 2002.
- Zhang, P., Wang, W., Zhang, T., Chen, L., Du, Y., Li, C., and Lv, J.: Theoretical study on the mechanism and kinetics for the self-reaction of $\text{C}_2\text{H}_5\text{O}_2$ radicals, *J. Phys. Chem. A*, 116, 4610–4620, <https://doi.org/10.1021/jp301308u>, 2012.
- Zhao, Y. and Truhlar, D. G.: A new local density functional for main-group thermochemistry, transition metal bonding, thermochemical kinetics, and noncovalent interactions, *J. Chem. Phys.*, 125, 194101–194119, <https://doi.org/10.1063/1.2370993>, 2006.
- Zhao, Y. and Truhlar, D. G.: The M06 suite of density functionals for main group thermochemistry, thermochemical kinetics, noncovalent interactions, excited states, and transition elements: two new functionals and systematic testing of four M06-class functionals and 12 other functionals, *Theor. Chem. Acc.*, 120, 215–241, <https://doi.org/10.1007/s00214-007-0310-x>, 2008.
- Zheng, J. and Truhlar, D. G.: Direct dynamics study of hydrogen-transfer isomerization of 1-pentyl and 1-hexyl radicals, *J. Phys. Chem. A*, 113, 11919–11925, <https://doi.org/10.1021/jp903345x>, 2009.
- Zheng, J., Xu, X., and Truhlar, D. G.: Minimally augmented Karlsruhe basis sets, *Theor. Chem. Acc.*, 128, 295–305, <https://doi.org/10.1007/s00214-010-0846-z>, 2011.
- Zhong, J., Kumar, M., Francisco, J. S., and Zeng, X. C.: Insight into chemistry on cloud/aerosol water surfaces, *Accounts Chem. Res.*, 51, 1229–1237, <https://doi.org/10.1021/acs.accounts.8b00051>, 2018.
- Zhou, X., Liu, Y., Dong, W., and Yang, X.: Unimolecular reaction rate measurement of *syn*- CH_3CHOO , *J. Phys. Chem. Lett.*, 10, 4817–4821, <https://doi.org/10.1021/acs.jpcllett.9b01740>, 2019.
- Zhu, C., Kumar, M., Zhong, J., Li, L., Francisco, J. S., and Zeng, X. C.: New mechanistic pathways for Criegee-water chemistry at the air/water interface, *J. Am. Chem. Soc.*, 138, 11164–11169, <https://doi.org/10.1021/jacs.6b04338>, 2016.